Received: 18 November 2020 | Accepted: 30 November 2020

DOI: 10.1002/jnr.24775

RESEARCH ARTICLE

Gpr37l1/prosaposin receptor regulates Ptch1 trafficking, Shh production, and cell proliferation in cerebellar primary astrocytes

Gina La Sala[1] | Chiara Di Pietro[1] | Rafaele Matteoni[1] | Giulia Bolasco[2] | Daniela Marazziti[1] | Glauco P. Tocchini-Valentini[1]

[1]Institute of Biochemistry and Cell Biology, Italian National Research Council (CNR), Monterotondo Scalo, Rome, Italy

[2]Epigenetics and Neurobiology Unit, European Molecular Biology Laboratory (EMBL), Monterotondo Scalo, Rome, Italy

Correspondence
Daniela Marazziti, Institute of Biochemistry and Cell Biology, Italian National Research Council (CNR), Via E. Ramarini 32, I-00015 Monterotondo Scalo, Rome, Italy.
Email: daniela.marazziti@cnr.it

Funding information
European Commission; Consiglio Nazionale delle Ricerche

Abstract

Mammalian cerebellar astrocytes critically regulate the differentiation and maturation of neuronal Purkinje cells and granule precursors. The G protein-coupled receptor 37-like 1 (Gpr37l1) is expressed by Bergmann astrocytes and interacts with patched 1 (Ptch1) at peri-ciliary membranes. Cerebellar primary astrocyte cultures from wild-type and *Gpr37l1* null mutant mouse pups were established and studied. Primary cilia were produced by cultures of both genotypes, as well as Ptch1 and smoothened (Smo) components of the sonic hedgehog (Shh) mitogenic pathway. Compared to wild-type cells, *Gpr37l1*$^{-/-}$ astrocytes displayed striking increases in proliferative activity, Ptch1 protein expression and internalization, intracellular cholesterol content, ciliary localization of Smo, as well as a marked production of active Shh. Similar effects were reproduced by treating wild-type astrocytes with a putative prosaptide ligand of Gpr37l1. These findings indicate that Gpr37l1–Ptch1 interactions specifically regulate Ptch1 internalization and trafficking, with consequent stimulation of Shh production and activation of proliferative signaling.

KEYWORDS

cholesterol, G protein-coupled receptor, mouse mutant, primary cilium, RRID:AB_10709580, RRID:AB_10844948, RRID:AB_11000053, RRID:AB_11204167, RRID:AB_11205039, RRID:AB_141373, RRID:AB_141607, RRID:AB_141788, RRID:AB_162543, RRID:AB_1839970, RRID:AB_1904103, RRID:AB_2059853, RRID:AB_2060867, RRID:AB_2072166, RRID:AB_2109645, RRID:AB_2174039, RRID:AB_2174045, RRID:AB_2239686, RRID:AB_2245173, RRID:AB_2300649, RRID:AB_2534102, RRID:AB_2535792, RRID:AB_2536180, RRID:AB_2857918, RRID:AB_330744, RRID:AB_331646, RRID:AB_396365, RRID:AB_631728, RRID:AB_632416, RRID:AB_772207, RRID:AB_772210, RRID:AB_839154, RRID:AB_839504, RRID:MGI:5512669, RRID:SCR_002789, RRID:SCR_003070, RRID:SCR_003238, RRID:SCR_007370, RRID:SCR_010279, RRID:SCR_013673, RRID:SCR_014199, RRID:SCR_014210

Edited by Cristina Ghiani and David Mc Arthur. Reviewed by Walter Witke and Raul Estevez.

Gina La Sala and Chiara Di Pietro should be considered joint first authors.

Daniela Marazziti and Glauco P. Tocchini-Valentini should be considered joint senior authors.

1 | INTRODUCTION

Mammalian astrocytic glial cells present a variety of morphological and biochemical characteristics, as well as functional specializations, depending on their cerebral tissue- and developmental stage-specific localization and distribution (Buosi et al., 2018; Hu et al., 2019; Matyash & Kettenmann, 2010; Okuda, 2018). Different astrocyte types have been classified, according to the expression of specific subsets of membrane receptor and ion channel markers and the synthesis of various extracellular matrix components, as well as growth and other soluble factors, including some with potent neuro-proliferative, -protective, and -regenerative effects (Pinto et al., 2000).

Astrocytes' regulation of neuronal proliferation, differentiation, and function is advantageously studied in the cerebellar tissue, which presents a relatively limited set of specifically interacting, well-characterized neuronal and astrocytic types, including fibrous astrocytes of the white matter, cortical granular layer's bushy velate astrocytes, and Purkinje cell layer's polarized Bergmann glia (BG) cells (Buffo & Rossi, 2013; Farmer et al., 2016; Leto et al., 2016).

Cellular sensing and transduction of a large variety of molecular and mechanical extracellular stimuli are specifically enacted by the primary cilia (PC), cell surface protruding organelles with complex plasma membrane-microtubule organization (Singla & Reiter, 2006). Intracellular signaling cascades provoked by ciliary activity as well as their physiological or pathological alterations are distinctly tissue- and cell type dependent. In particular, PC are required for mammalian brain development, controlling the activation and modulation of specific neuronal mitogenic and developmental signals, such as those induced by sonic hedgehog (Shh)- and wingless type-dependent pathways (Gerdes et al., 2007; Han et al., 2008).

Several studies have shown a crucial role played by PC during cerebellar development (Chizhikov et al., 2007; Di Pietro et al., 2017; Spassky et al., 2008). During the earliest postnatal stages the proliferation of neuronal granule cell progenitors (GCPs) in the external granule layer specifically requires the secretion of Shh by Purkinje neurons. Shh proliferative signals are regulated by several factors and require the interaction between Shh and patched 1 (Ptch1) co-receptor complex (Allen et al., 2011; Izzi et al., 2011). Binding of Shh to the Ptch1 complex leads to ciliary translocation and derepression of the membrane effector smoothened (Smo), thus triggering the transcriptional activation of several proliferation-related genes (Ho & Scott, 2002).

Shh also promotes the postnatal proliferation and maturation/differentiation of murine cerebellar BG astrocytes (Dahmane & Ruiz, 1999; Di Pietro et al., 2017), which produce PC from P0 to adulthood (Di Pietro et al., 2017; Marazziti et al., 2013), as well as high levels of Ptch1- and glioma-associated oncogene-Kruppel family (Gli) transcription factors (Traiffort et al., 2002; Wallace & Raff, 1999). Patched 2 and Smo proteins are also specifically expressed by cultured glutamate aspartate transporter (Glast)-positive cerebellar astrocytes (Okuda et al., 2016).

Shh addition to cultured cerebellar samples also induces BG differentiation (Dahmane & Ruiz, 1999) but the detailed mechanisms of Shh-mediated effects on astrocytes have not yet been clarified (De Luca et al., 2016; Farmer et al., 2016; Farmer & Murai, 2017).

Significance

The sonic hedgehog (Shh) secreted lipoprotein crucially regulates cell proliferation and organ morphogenesis at all stages of development and differentiation in vertebrates. Shh signals are transduced within the cell and tune the expression of many genes which control cellular replication. This requires the Shh-induced activation of patched 1 (Ptch1) and smoothened membrane proteins, at specialized, cell-protruding organelles (primary cilia). This study highlights the specific role of the G protein-coupled receptor 37-like 1, another peri-ciliary, Ptch1-interacting protein, in regulating Shh proliferative signals in early postnatal mouse cerebellar astrocytic cells, which in turn critically modulate the differentiation and maturation of cerebellar neurons.

Several members of the G protein-coupled receptor (GPR) protein superfamily are emerging as important regulators of ciliogenesis (Pedersen et al., 2016). For example, in the absence of Shh stimulation, the orphan Gpr161 protein is preferentially located at PC where it promotes the production of cyclic AMP (cAMP) and stimulation of protein kinase A, leading to proteolytic cleavage of Gli transcription factors into their repressor forms (GLI-R). Shh-, Ptch1-induced ciliary translocation of Smo also triggers exit of Gpr161 from PC, which results in a local decrease in cAMP concentration and stabilization of full-length Gli activator forms (GLI-A). Furthermore, functional studies on another orphan receptor, Gpr175, revealed its activation of G protein inhibitory α-subunits ($G\alpha_i$) transduction at periciliary membranes, with lowering of cAMP levels and enhancement of Shh-mediated signaling (Singh et al., 2015).

The vertebrate G protein-coupled receptor 37 and G protein-coupled receptor 37-like 1 (*GPR37* and *GPR37L1*) genes encode 7-transmembrane span proteins with amino acid sequence homology to GPRs for the endothelin and bombesin peptides (Marazziti et al., 1997, 1998; Valdenaire et al., 1998). The neuro-and glio-protective prosaposin proteins and derived prosaptide analogs have been proposed as possible ligands of both putative receptors, causing their internalization and specific activation of intracellular signaling mediated by $G\alpha_i$ proteins, in primary rat astrocytes as well as certain cultured cell expression systems (Liu et al., 2018; Lundius et al., 2014; Meyer et al., 2013, 2014; Smith, 2015).

Mammalian GPR37L1 proteins are specifically expressed in cerebellar BG astrocytes and take part in regulating postnatal cerebellar granule neuron proliferation-differentiation, and BG and Purkinje neuron maturation. The murine Gpr37l1 protein co-localizes and interacts with Ptch1 in peri-ciliary membranes of BG cells. Mouse null mutants for the *Gpr37l1* gene exhibit a precocious termination of

postnatal cerebellar development and maturation and these effects are linked to an overall dysregulation of Shh–Ptch1–Smo signaling (Di Pietro et al., 2017; Marazziti et al., 2013).

The present study aimed at elucidating the function of the Shh signaling pathway in *ex vivo* cultures of murine primary astrocytes derived from the cerebellar cortex of *Gpr37l1* null murine mutants. Following the ultrastructural identification of PC in BG cells from wild-type mouse samples, cerebellar primary astrocytes were prepared and cultured from both wild-type and *Gpr37l1*$^{-/-}$ pups. PC were similarly produced by cultured cells of both genotypes. Cellular proliferation and intracellular trafficking of mitogenic pathway and PC components were then studied, upon stimulation with Shh, with a Smo antagonist and proliferation inhibitor, SANT-1 and with the prosaptide ligand, TX14(A) (Liu et al., 2017; Meyer et al., 2013, 2014).

Compared to wild-type cultures, *Gpr37l1*$^{-/-}$ cerebellar astrocytes display a markedly increased proliferative activity, higher expression of the Ptch1 protein and augmented intracellular cholesterol content, with the associated increase in Ptch1 internalization and Smo localization at PC. Noticeably, *Gpr37l1*$^{-/-}$ astrocytes also produce and secrete active Shh, in much higher amounts compared to wild-type cells. Consistent with these findings treatment of wild-type astrocytes with the TX14(A) prosaptide, led to a ligand-induced co-internalization of the Gpr37l1 and Ptch1 proteins.

Overall, these findings support a model in which the Gpr37l1–Ptch1 interaction critically regulates the Shh mitogenic pathway in cerebellar astrocytes. Gpr37l1 modulates Ptch1 internalization and trafficking to endosomal compartments and, consequently, Shh production and secretion, ciliary translocation of Smo and activation of proliferative signaling cascades.

2 | MATERIALS AND METHODS

2.1 | Mice

Heterozygous and homozygous *Gpr37l1* knock-out mutant, male and female mice and their wild-type littermates were used (*Gpr37l1*$^{+/-}$, *Gpr37l1*$^{-/-}$ and *Gpr37l1*$^{+/+}$, RRID:MGI:5512669). All mice were bred from heterozygous crossings, following backcrossing onto a wild-type C57BL/6J background for 10 generations and used as previously described (Marazziti et al., 2013). After weaning, mice were housed by litter of the same sex, 3–5 per cage, and maintained in a temperature-controlled room at 21 ± 2°C, on a 12-hr light–dark cycle (lights on at 07:00 a.m.), with food and water available ad libitum. All animals were born and bred in a specific pathogen-free facility and were subjected to experimental protocols, as reviewed and approved by the Ethical and Scientific Commission of Veterinary Department of the Italian Ministry of Health, according to the ethical and safety rules and guidelines for the use of animals in biomedical research provided by the Italian laws and regulations, in application of the relevant European Union's directives (no. 86/609/EEC and 2010/63/EU).

2.2 | Transmission electron microscopy

Adult (3 months) mice organs were fixed by intracardial perfusion with 2% paraformaldehyde (PFA) and 2.5% glutaraldehyde. Brains were postfixed in 2.5% glutaraldehyde overnight at 4°C, cut sagittaly at 300 μm, and processed for electron microscopy as described previously (Doetsch et al., 1997). Briefly, sections were postfixed in 2% osmium tetroxide in 0.1 M phosphate buffer (pH 7.2) for 2 hr. Semi-thin sections, 1.5 μm thick, were cut with a diamond knife and stained with 1% toluidine blue. For the identification of PC, 300 ultrathin (0.05 μm) serial sections were collected in slot grids covered with Formvar resin (Sigma-Aldrich-Merck, Cat# 09823) counterstained with uranyl acetate and lead citrate, and analyzed in a Jeol JEM-1010 electron microscope (JEOL USA Inc.). Pictures were taken with a Gatan MSC 791 CCD digital camera (Gatan) and programmatically adjusted for brightness and contrast using Adobe Photoshop CS software (RRID:SCR_014199).

2.3 | Cerebellar astrocyte culture and treatments

Primary astrocytes cultures were prepared from the pooled cerebella of 7–8 *Gpr37l1*$^{+/+}$ or *Gpr37l1*$^{-/-}$ male or female mouse pups (WT and KO primary cultures) by a modification of a previously described method (Hatten, 1985). A total of about 150 mouse pups per genotype were used. Each cerebellar pool initially comprised ca. 2–3 × 10^6 cells of same genotype, to be expanded for use in each experimental analysis. Briefly, cerebella from postnatal day 7 (P7) pups were dissected, cut into small pieces and incubated for 10 min at 37°C, with trypsin (Sigma-Aldrich, Cat# T6763; 10 mg/ml) and deoxyribonuclease I (DNAse I; Sigma-Aldrich, Cat# D4527; 1 mg/ml) in Hanks' balanced salt solution (HBSS; GE Healthcare Life Sciences, Cat# SH30368.01). Cell suspensions were washed for three times with Dulbecco's Modified Eagle Medium (DMEM; EuroClone, Cat# ECM0728L), containing 10% fetal bovine serum (FBS; Gibco, Cat# 10270106), 2 mM L-glutamine (Gibco, Cat# 25030024), 50 U/ml penicillin-streptomycin (Gibco, Cat# 15070-063 5,000 U/ml), and pre-plated on an uncoated 6-well plate (EuroClone, Cat# ET3006) for 1 hr to remove contaminant fibroblasts. Unattached cells were transferred for 1 hr on poly-L-lysine-coated (0.1 mg/ml; Sigma-Aldrich, Cat# P1399) 24-well plates (0.5 ml/well; Costar, Cat# 3524) or 6-well plates (2 ml/well) to allow astroglial cell attachment. After 1h cells were rinsed several times with 1× Dulbecco's phosphate-buffered saline (DPBS; Gibco, Cat# 14040091) to remove contaminant neurons and cultured at low density to avoid direct cell–cell contact, in DMEM containing 10% FBS serum, at 37°C and 5% CO_2. The medium was changed after 24 hr and adhering cells were cultured for 3–5 days in the same conditions, before splitting with trypsin (0.5 mg/ml) in 1× DPBS and plating on poly-L-lysine-coated culture plates.

Cells at ca. 70% confluence were starved for 24 hr in serum-free DMEM and then treated for 24 hr with the recombinant mouse sonic hedgehog (C25II) N-terminus (Shh-N; 100 nM; R&D System,

Cat# 464-SH-200), or the prosaptide ligand TX14(A) (100 nM; Eurogentec, Cat# AS-60248-1), or the Smo inhibitor SANT-1 (100 nM; Calbiochem, Cat# 559303), or with a combination of either 100 nM Shh-N and 100 nM TX14(X) or 100 nM SANT-1 and 100 nM TX14(X). For the latter treatment cells were pre-incubated for 1 hr with SANT-1 prior to the addition of TX14(X). Equal volumes of vehicle alone were added to the untreated cell samples. All treatments were administered with cells maintained in serum-free DMEM at 37°C and 5% CO_2. The above reagents were dissolved as follows: Shh-N in 1× DPBS, pH 7.4; TX14(A) in a binding assay buffer with protease inhibitors (Meyer et al., 2013); SANT-1 in dimethyl sulfoxide (DMSO; Sigma-Aldrich, Cat# D2650).

2.4 | Antigens and antibodies used for immunofluorescence labeling

The following primary antibodies were used as specific tissue/cell type markers and have extensive published data supporting their validity (Table 1): aquaporin 4 (Aqp4; 1:50, Santa Cruz, RRID:AB_2059853); ADP-ribosylation factor-like protein 13B (Arl13B; 1:500, UC Davis/NIH NeuroMab Facility, RRID:AB_11000053; 1:1,000, Proteintech, RRID:AB_2060867); caveolin 1 (1:50, Cell Signaling Technology, RRID:AB_2072166); contactin 2 (Cntn2/Tag1; 1:100, R&D Systems, RRID:AB_2245173); glial fibrillary acidic protein (Gfap; 1:500, Millipore, RRID:AB_2109645; 1:500, BD Biosciences Pharmingen, RRID:AB_396365); glial high affinity glutamate transporter (or glutamate aspartate transporter, Glast; 1:100, Novus Biologicals, RRID:AB_839154); Gpr37l1 (1:50, Mab Technologies, RRID:AB_2857918); ionized calcium binding adaptor molecule 1 (Iba1; 1:500, FUJIFILM Wako Chemicals, RRID:AB_839504); oligodendrocyte transcription factor 2 (Olig2; 1:1,000, Abcam, RRID:AB_11205039); Shh-E1 (1:400, Santa Cruz Biotechnology, RRID:AB_10709580); smoothened (Smo; 1:50, Santa Cruz, RRID:AB_2239686); patched 1 (Ptch1; 1:50, Santa Cruz, RRID:AB_2174039); RAB5A, member RAS oncogene family (Rab5a or Rab5; 1:200, Cell Signaling Technology, RRID:AB_2300649); RAB7, member RAS oncogene family (Rab7; 1:200, Cell Signaling Technology, RRID:AB_1904103); Alexa Fluorophore-conjugated secondary antibodies made in donkey (1:500, Invitrogen, specific for: rat, Cat# A11006 RRID:AB_141373; mouse, Cat# A21202 RRID:AB_141607 and Cat# A31570 RRID:AB_2536180; goat Cat# A11055 RRID:AB_2534102 and Cat# A21432 RRID:AB_141788; rabbit, Cat# A21206 RRID:AB_2535792 and Cat# A31572 RRID:AB_162543). The immunostaining of each marker showed the expected pattern of cellular morphology.

TABLE 1 List of used antibodies in immunohistochemistry and Western blot analysis

Name	Company	Species	Cat. Number	Use	RRID	Dilution
Aqp4	Santa Cruz	Goat; pAB	sc-9888	IHC	AB_2059853	1:50
Arl13b	NeuroMab	Mouse; mAB	73-287	IHC	AB_11000053	1:500
Arl13b	Proteintech	Rabbit; pAB	17711-1-AP	IHC	AB_2060867	1:1,000
Caveolin 1	Cell Signaling	Rabbit; pAB	3238	IHC	AB_2072166	1:50
Cntn2/Tag1	R&D Systems	Rabbit; pAB	AF1714	IHC	AB_2109645	1:100
Gfap	Millipore	Rabbit; pAB	AB5804	IHC	AB_2109645	1:500
Gfap	BD Biosci. Pharmingen	Mouse; mAB	556327	IHC	AB_396365	1:500
Glast	Novus Biologicals	Rabbit; pAB	NB110-55631	IHC	AB_839154	1:100
Gpr37l1	Mab Technologies	Mouse; mAB	scB12	IHC	AB_2857918	1:50
Gpr37l1	Santa Cruz	Goat; pAB	sc-164532	WB	AB_10844948	1:500
Iba1	Wako Chemicals	Rabbit; pAB	019-19741	IHC	AB_839504	1:500
Shh (E-1)	Santa Cruz	Mouse; mAB	sc-365112	IHC	AB_10709580	1:400
Shh (N-19)	Santa Cruz	Goat; pAB	sc-1194	WB	AB_632416	1:400
Smo	Santa Cruz	Mouse; mAB	sc-166685	IHC	AB_2239686	1:50
Olig2	Millipore	Mouse; mAB	MABN50A4	IHC	AB_11205039	1:100
p44/p42 Mapk	Cell Signaling	Rabbit: pAB	9102	WB	AB_330744	1:1,000
phospho-p44/p42 Mapk	Cell Signaling	Rabbit: pAB	9101	WB	AB_331646	1:1,000
Ptch1	R&D Systems	Rat; mAB	MAB41051	WB	AB_2174045	1:1,000
Ptch1 (G-19)	Santa Cruz	Goat; pAB	sc-6149	IHC	AB_2174039	1:50
Rab5	Cell Signaling	Rabbit; mAB	3547	IHC	AB_2300649	1:200
Rab7	Cell Signaling	Rabbit; mAB	9367	IHC	AB_1904103	1:200
α-tubulin	Sigma-Aldrich	Mouse; mAB	MABT205	WB	AB_11204167	1:1,000

Abbreviations: IHC, immunohistochemistry; mAB, monoclonal antibody; pAB, polyclonal antibody; WB, Western blot.

2.5 | Immunofluorescence labeling, microscopy, and quantitative image analysis

Primary astrocytes from WT and KO cultures were grown on poly-L-lysine-coated glass coverslips in 24-well plates. After treatments, the cells were kept at room temperature and fixed with 4% paraformaldehyde (PFA; Sigma-Aldrich, Cat# 158127) in DPBS for 15 min, permeabilized with 0.1% Triton X-100 (Merck, Cat# 108603) for 10 min and incubated for 1 hr in blocking buffer containing 20% normal donkey serum (Millipore, Cat# S30), 1% bovine serum albumin (BSA; Sigma-Aldrich, Cat# A4503) and 0.05% Tween-20 (Bio-Rad Laboratories, Cat# 1706531). Samples were then incubated overnight at 4°C, with primary antibodies diluted in blocking buffer, followed by washing and incubation with fluorophores-conjugated secondary antibodies. Nuclei were stained with 4,6-diamino-2-phenylindole (DAPI; Molecular Probes, Cat# D1306).

Gpr37l1 immunostaining was performed as above, after fixing the cells with 100% methanol at −20°C for 20 min, permeabilizing with 0.1% Triton X-100 and incubating for 1 hr at room temperature in blocking buffer containing 0.5% BSA, 0.3 M Glycine (Merck, Cat# 104201) and 0.1% Tween-20.

Fluorescence micrographs were acquired with a TCS SP5 laser scanning confocal microscope or with a motorized LMD7000 microscope (Leica Microsystems) using the manufacturer's imaging software. The percentage of Gfap-positive ciliated cells was assessed by fluorescence microscopy-based visualization of Arl13b-stained PC and DAPI-labeled nuclei. The percentage of cells with Smo localized in PC was assessed by counting the total number of Gfap-positive ciliated cells with also Smo-positive cilia. Images were analyzed by ImageJ software (NIH, RRID:SCR_003070). For each sample at least 20 fields were counted. Images were scored blinded before quantification.

The colocalization analysis was performed using the specific threshold plug-in of FiJi-ImageJ software v2.1.0/1.53c (NIH, RRID:SCR_003070). Colocalization of Ptch1 and Rab7 was evaluated upon measurement of Pearson's correlation coefficient, based on the pixel intensity correlation over space. For each multichannel acquired image, the analysis was performed on manually chosen regions of interest (ROI), each selected within one cell. At least 10 ROIs per experimental group with at least three samples per genotype were analyzed. Images were scored blinded before quantification.

2.6 | RNA extraction and real-time PCR assay

Total RNA was extracted from WT and KO primary cultures (ca. 1×10^6 cells) or frozen whole brain samples (1 mg) from wild-type, *Gpr37l1*$^{-/-}$ and *Gpr37*$^{-/-}$ (Marazziti et al., 2004) adult mice, using a RNeasy Plus Mini kit (QIAGEN, Cat# 74134) according to the manufacturer's instructions. Total RNA preparations were reverse-transcribed according to standard procedures. Real-time PCR (RT-PCR) was performed using the following primers: mouse Gpr37l1, forward 5′-GGCAATCTGTCTGTCATGTG-3′ and reverse 5′-CACATGGAATCGGTCTATGC-3′; mouse Gpr37, forward 5′-AGAGCTGGAGCTGTCGCCC-3′ and reverse 5′-GGCCTGC CTTCAATATACA-3′ (Marazziti et al., 2004). Experiments were repeated at least three times, and samples were analyzed in triplicate.

2.7 | Cell proliferation assay

Cell proliferation was determined by 5-bromo-2′-deoxyuridine (BrdU, Sigma-Aldrich, Cat# B5002) incorporation experiments. WT and KO cultures were plated on poly-L-lysine-coated glass coverslips in 24-well plates and grown as previously described. Cells at ca. 70% confluence were starved for 24 hr in serum-free DMEM and then treated with either Shh-N or TX14(A) at different concentrations (10, 100, or 200 nM and 10, 100, or 1,000 nM, respectively) or vehicle for 24 hr, in serum-free DMEM, at 37°C and 5% CO_2. Other cell samples were starved for 24 hr with serum-free DMEM and then treated as described above, with either 100 nM Shh-N, 100 nM SANT-1, 100 nM TX14(A) or their combinations, or vehicle for 24 hr, in serum-free DMEM. All treated cells were pulsed with 10 μM BrdU for the last 16 hr during each treatment period and then fixed and co-stained with anti-BrdU and anti-GFAP according to standard protocols (Marazziti et al., 2013).

At least 500 BrdU-positive cells per experimental condition were quantified using the ImageJ software in three or more independent experiments. Experiments were repeated at least three times with different cell culture preparations, and samples were analyzed in triplicate in a blinded manner.

2.8 | Filipin staining and analysis of free intracellular cholesterol levels

Filipin staining was applied for analyzing free intracellular cholesterol levels (Muller et al., 1984). Primary astrocytes were grown on glass coverslips, fixed with 4% paraformaldehyde solution in DPBS, incubated for 20 min at room temperature with ammonium chloride (20 mM) in DPBS, and blocked and permeabilized in 1× DPBS, 0.2% Triton X-100 solution. After Gfap immunostaining (1:500, BD Biosciences Pharmingen; RRID:AB_396365), cells were incubated overnight at 4°C, with filipin (50 μg/ml; Sigma-Aldrich, Cat# F4767) in DPBS. Excess filipin was removed by washing with cold DPBS and fluorescence images were immediately captured using a TCS SP5 laser scanning confocal microscope (Leica Microsystems), with ultraviolet excitation around 360 nm and emission detection around 450 nm, using manufacturer's imaging software. All procedures were carried out with complete protection from ambient light. Filipin staining intensity was quantified with Imaris Standard Package for OLME Systems, v7.1 (Bitplane, RRID:SCR_007370). For each acquired image, the analysis was performed on manually selected ROI, each corresponding to one cell. At least 10 ROIs per experimental group with at least three samples per genotype were analyzed. Images were scored blinded before quantification.

2.9 | Protein extraction and Western blot analysis

Protein extracts were prepared from WT and KO primary astrocytes, after culture in control conditions or after serum starvation followed by treatment for 24 hr with Shh-*N* (100 nM) or TX14(A) (100 nM), or from striata of wild-type or *Gpr37*$^{-/-}$ adult mice (Marazziti et al., 2004). Cell and tissue samples were dissolved in lysis buffer (20 mM HEPES pH 7.3, 120 mM NaCl, 5 mM EDTA, 10% glycerol, 1% Triton X-100, Roche complete protease inhibitor cocktail) and cleared by centrifugation. The protein content of supernatant was quantified by detergent-compatible assay (Bio-Rad) and protein samples (50 μg) were separated by SDS-PAGE and analyzed by Western blot, according to standard protocols. Protein antigens were immunodetected with the following primary antibodies, which labeled the respective protein bands of expected molecular weight as reported in previous publications: Ptch1 (1:1,000, R&D Systems, RRID:AB_2174045), Gpr37l1 (1:500, Santa Cruz, RRID:AB_10844948); Gpr37 (clone #202, 1:1,000, kindly provided by R. Takahashi and Y. Imai, RIKEN Brain Science Institute, Saitama, Japan); Shh-N19 (1:400, Santa Cruz, RRID:AB_632416); α-tubulin (1:1,000, Sigma-Aldrich, RRID:AB_11204167). Horseradish peroxidase-conjugated secondary antibodies, specific for rat (Amersham Biosciences-GE Healthcare, Cat# NA935 RRID:AB_772207) mouse (Amersham Biosciences-GE Healthcare, Cat# NA931 RRID:AB_772210), goat (Santa Cruz, Cat# sc-2020, RRID:AB_631728) immunoglobulins were used, following the producer's instructions. The blotted membranes were then processed for chemiluminescence detection with an ECL kit (Amersham, Cat# GEHRPN2232) and exposed (Chemidoc XRS+ imager, Bio-Rad, RRID:SCR_014210). The luminescent signal of immunoreactive bands was imaged and quantified with the Image Lab software (Bio-Rad, RRID:SCR_014210). The intensity of each band was normalized to the intensity of the corresponding α-tubulin band. The average values of each experimental group were expressed in arbitrary units, as a ratio to the mean values obtained from the wild-type control group.

2.10 | Analysis of mitogen-activated protein kinase phosphorylation levels

Cultured primary astrocytes were starved for 3 hr in serum-free DMEM at 37°C and 5% CO_2 before analysis. About 1×10^6 cells for each sample were rapidly harvested in lysis buffer (62.5 mM Tris·HCl pH 6.8, 25% glycerol, 2% SDS and 0.01% bromophenol blue), sonicated and processed for Western blot analysis, as described above, with polyclonal antibodies specific for mitogen-activated protein kinase 3/1 (Mapk3/1 or Erk1/2 or p44/p42 Mapk; 1:1,000, Cell Signaling Technologies, RRID:AB_330744, Table 1) or Thr202/Tyr204 phosphorylated Mapk3/1 (phospho-Mapk3/1 or phospho-p44/p42 Mapk; 1:1,000, Cell Signaling Technologies, RRID:AB_331646, Table 1). The data shown in the figure are representative of three to five independent experiments. Experimental results were scored blinded to genotype and analyzed by unpaired *t* test. *P* values less than 0.05 were considered significant.

2.11 | Conditioned medium assay and analysis

Cultures of WT and KO primary astrocytes were seeded into 24-well plates and allowed to reach ca. 80% confluence. Following starvation in serum-free DMEM for 24 hr, conditioned medium (CM) samples were collected. CM from either WT or KO cultures was added to other sets of WT cells, after they had been subjected to serum starvation for 24 hr. A Shh-specific monoclonal antibody (E1; Santa Cruz; RRID:AB_10709580) or anti-mouse immunoglobulins G (Sigma-Aldrich, Cat. #M-9902, RRID:AB_1839970) were added (final concentration 2.5 μg/ml), as indicated. After 24 hr of incubation in serum-free medium at 37°C and 5% CO_2, BrdU incorporation or Western blot assays were performed, as reported above.

Proteins in CM samples (5 ml) from WT or KO cultures were concentrated by Vivaspin Turbo 4 protein concentrator spin columns (Sartorius AG, Cat. #VS04T01), separated by SDS-PAGE and analyzed by Western blot, according to standard protocols.

2.12 | TUNEL assay

The presence of apoptotic cells in WT or KO cultures was tested by terminal deoxynucleotidyl transferase-mediated dUTP nick end labeling (TUNEL) assay with In Situ Cell Death Detection Kit **(**Merck, Cat# 12156792910**)**. Fluorescence micrographs were acquired with a LMD7000 motorized microscope.

2.13 | Figure composition

Figures were composed in Adobe Illustrator CS (Adobe, RRID:SCR_010279). For representative confocal images, maximum projections of more than 10 *z*-stacks were generated with Leica Application Suite X (RRID:SCR_013673). Images were adjusted for brightness and contrast using Adobe Photoshop CS software.

2.14 | Statistical analysis

GraphPad Prism version 5.0 (Graph Pad, RRID:SCR_002789) was used for statistical analysis of the data. All analyzed samples were obtained from at least seven individual pups for each experimental condition, in agreement with specific sample size analysis for standardized comparison of murine mutant phenotypes, as reported by the reference European Mouse Disease Clinic Consortium (EUMODIC) and International Mouse Phenotyping Consortium (IMPC) (Hrabe de Angelis, 2015; Meehan et al., 2017).

All data are presented as mean ± standard deviation (*SD*). All experimental data were included in the results. Experimental results

were scored blinded and one-way analysis of variance (ANOVA) with Bonferroni post hoc test, was used to determine statistical significance for experiments with three or more experimental groups. The effects of the two studied genotypes on Mapk phosphorylation levels were analyzed by unpaired *t* test. *P* values of less than 0.05 were considered significant. Statistical details are reported in each figure legend.

3 | RESULTS

3.1 | Primary cilia in mouse cerebellar Bergmann astrocytes

PC-like projections were previously described in mammalian cerebral cortical astrocytes, as well as cultured hippocampal neurons and astrocytes (Berbari et al., 2007; Bishop et al., 2007). The present study originally provides the specific ultrastructural identification and characterization of PC in mouse BG astrocytes upon electron microscopy and morphological analysis of cerebella from wild-type, C57BL/6J congenic adult animals (Figure 1). This confirms previous immunolabeling results (Di Pietro et al., 2017; Marazziti et al., 2013) and highlights the importance of specifically studying the presence and function of PC in BG-derived cultured cerebellar astrocytes.

3.2 | Production and characterization of *Gpr37l1*$^{+/+}$ and *Gpr37l1*$^{-/-}$ mouse cerebellar primary astrocytes

Ciliogenesis-competent murine cerebellar primary astrocytes were cultured and used to study Gpr37l1's modulation of Shh-induced

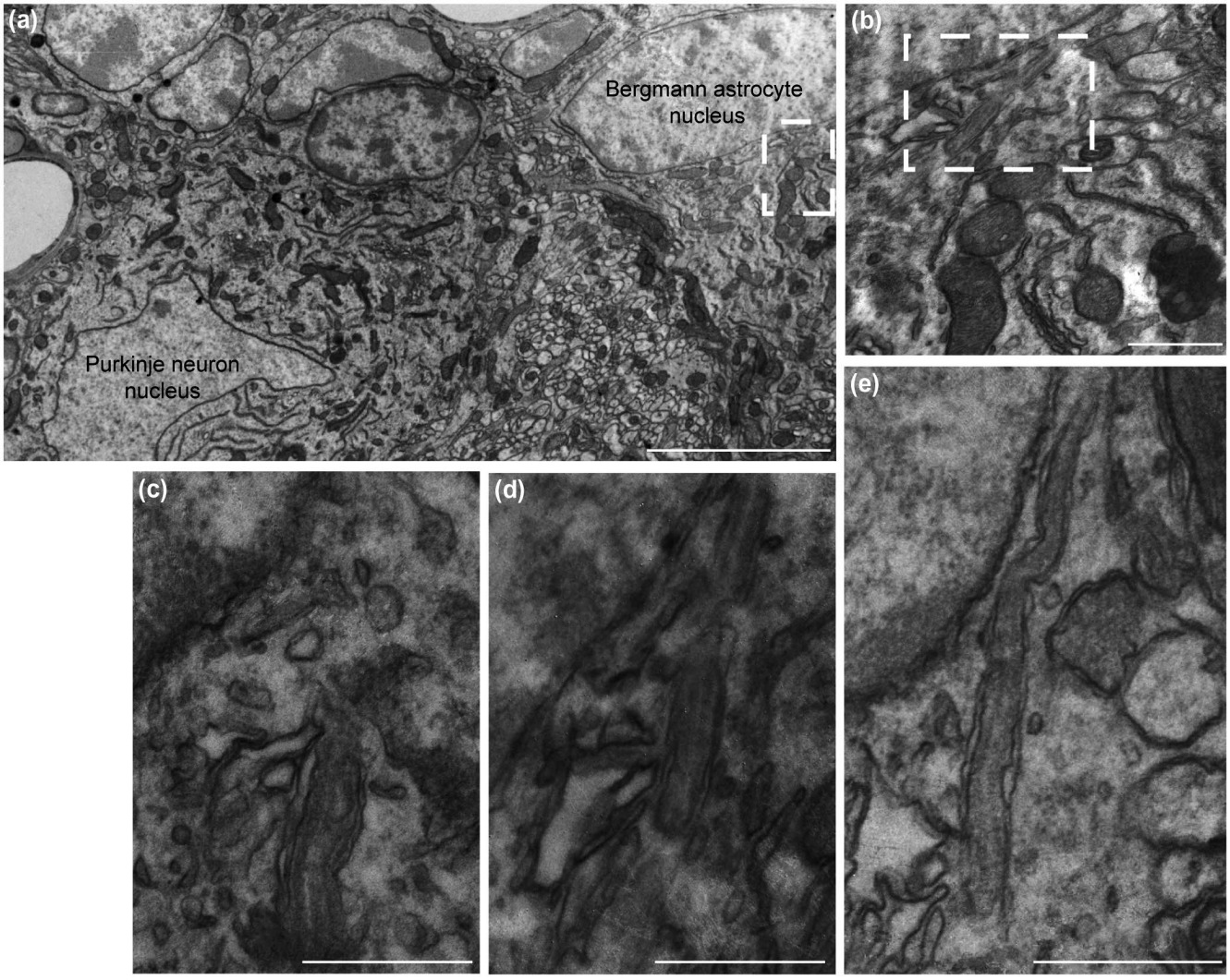

FIGURE 1 Ultrastructural analysis of primary cilium in mouse Bergmann glia astrocytes. (a) Low magnification transmission electron microscopy image of the Purkinje cell layer in an adult mouse cerebellum. Both Purkinje neuron and Bergmann glia (BG) astrocyte nuclei are indicated, according to their reported characterization (Palay & Chan-Palay, 1974). Scale bar: 5 μm. (b) Higher magnification image of boxed area in panel a, showing a PC within the BG astrocyte's perinuclear area which appears sagittal to the plane of sectioning. The same PC is shown in subsequent serial sections (50 nm-spaced) in panels c, d and e. Scale bar: 0.5 μm

mitogenic. Homogeneous monolayers of mouse primary astrocytes were derived as previously described (Yoshimura et al., 2011), from cerebella of P7 *Gpr37l1*$^{+/+}$ and *Gpr37l1*$^{-/-}$ littermates (WT and KO astrocytes). All pups originated from crossing of heterozygous animals of the original C57BL/6J congenic strain, which shows increasing cerebellar expression of the Gpr37l1 protein from P5 to P15 (Marazziti et al., 2013). Astrocyte cultures at sub-confluent conditions were subjected to serum starvation, to induce cell-cycling arrest and entering in G0 phase and to stimulate the formation of PC (Kiprilov et al., 2008; Ott & Lippincott-Schwartz, 2012; Zhang et al., 2009). Serum removal was applied to also deplete exogenous mitogens and other soluble effectors in the culture medium (Liu et al., 2018).

Serum-starved cultures were then characterized by immunofluorescence labeling with antibodies against various astrocyte markers, including Gpr37l1, and the PC marker, Arl13b (Figures 2 and S1).

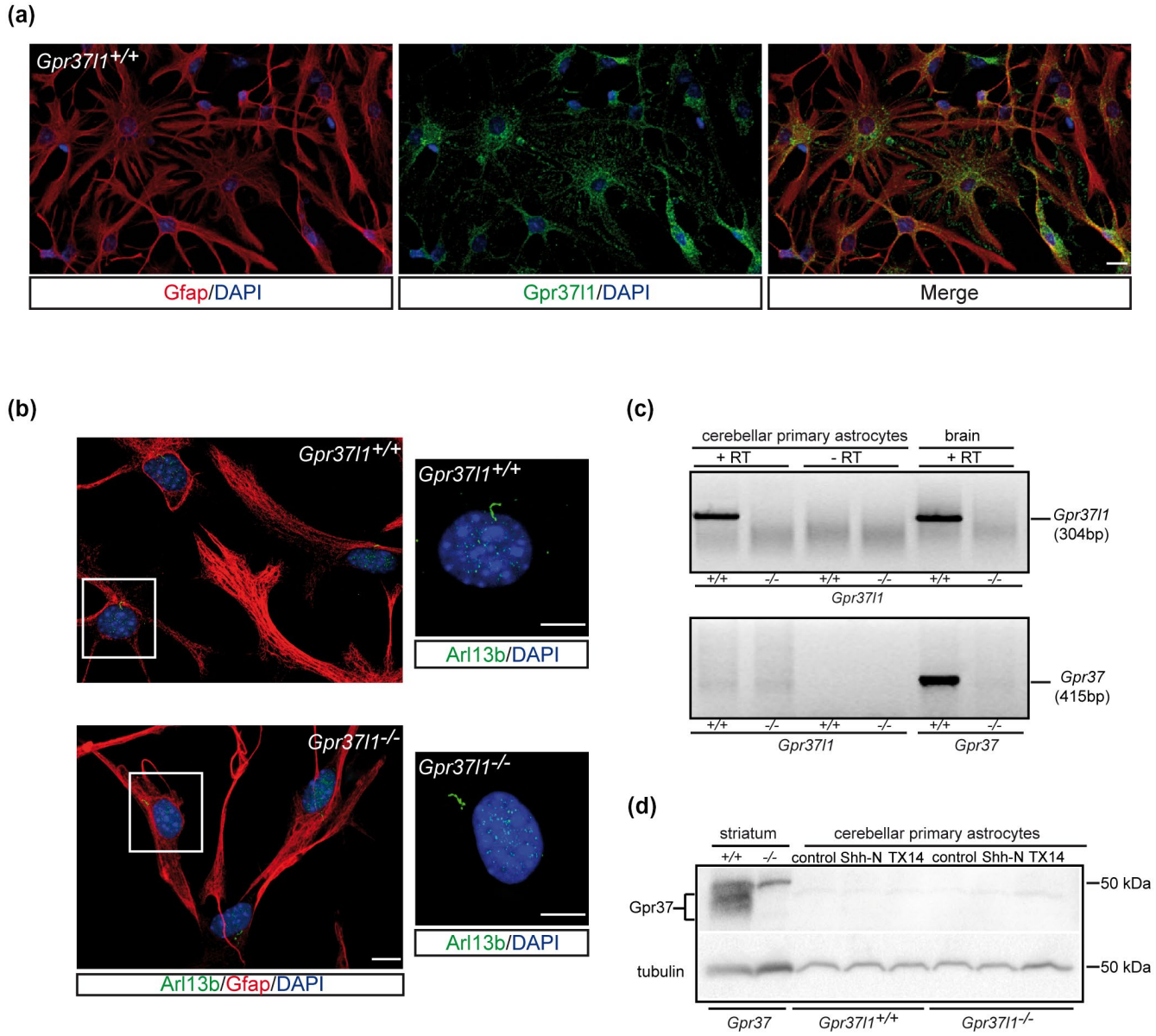

FIGURE 2 Gpr37l1 is expressed in cultured mouse cerebellar astrocytes. (a) Representative confocal images of Gfap (red) or Gpr37l1 (green) immunofluorescence labeling and DAPI nuclear staining (blue) in serum-starved, cultured cerebellar astrocytes from *Gpr37l1*$^{+/+}$ pups. Scale bar: 20 μm. (b) Representative confocal images of Gfap (red) and Arl13b (green) co-immunofluorescence labeling and DAPI staining (blue) in serum-starved, cultured cerebellar astrocytes from *Gpr37l1*$^{+/+}$ or *Gpr37l1*$^{-/-}$ pups. Higher magnifications of boxed areas with Arl13b-positive PC (green) and DAPI staining (blue) are shown in the right panels. Scale bars: 10 μm. (c) RT-PCR analysis of Gpr37l1 (upper panel) or Gpr37 (lower panel) mRNA expression in mouse cultured cerebellar astrocytes or whole brain samples. Total RNA was extracted from *Gpr37l1*$^{+/+}$ or *Gpr37l1*$^{-/-}$ pup's cultured cerebellar astrocytes or frozen whole brain samples from wild-type, *Gpr37l1*$^{-/-}$ or *Gpr37*$^{-/-}$ adult mice. (d) Representative Western blot of Gpr37 protein levels in striatum tissue extracts from *Gpr37*$^{+/+}$ or *Gpr37*$^{-/-}$ adult mice and lysates of cerebellar primary astrocytes from *Gpr37l1*$^{+/+}$ or *Gpr37l1*$^{-/-}$ pups, after serum starvation followed by treatment with control vehicle, or Shh-N, or TX14(A) [Color figure can be viewed at wileyonlinelibrary.com]

About 90% of all cells were positively stained for astrocyte-specific marker, Gfap. All Gfap-positive cells also showed specific Gpr37l1 immunostaining (Figure 2a). There was no difference between WT and KO cultures in the expression of Gfap or the other glial markers, high-affinity glutamate transporter (Glast) and water transporter aquaporin 4 (Aqp4) (Figures 2b and S1a,b). Cells positive for the oligodendrocyte progenitor transcription factor 2 (Olig2) or the postmitotic granule neuron contactin 2 (Cntn2 or Tag1) markers were very rare, while about 10% of cells were positive for the microglial marker, allograft inflammatory factor 1 (or ionized calcium binding adaptor molecule 1, Iba1) (Figure S1c). Two predominant forms of astrocytes were present: stellate and bi-tripolar cells (Mason, 1988), in a proportion of about 85% to 15% in WT and 70% to 30% in KO cultures (Figure S1d). Astrogliosis (Eddleston & Mucke, 1993;

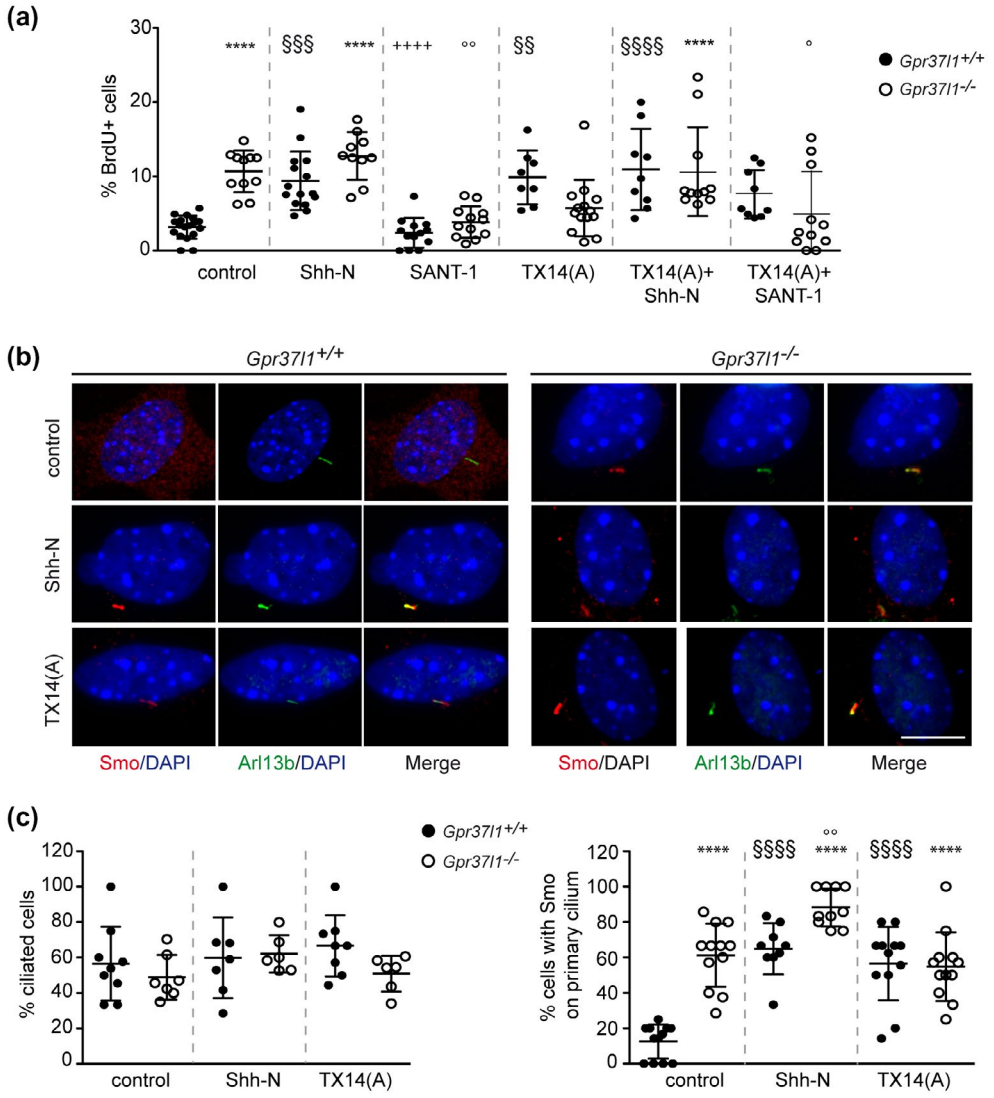

FIGURE 3 Cell proliferation and Smo localization in cerebellar primary astrocytes from *Gpr37l1*$^{+/+}$ or *Gpr37l1*$^{-/-}$ pups. (a) BrdU incorporation was quantified in serum-starved cerebellar primary astrocytes from *Gpr37l1*$^{+/+}$ or *Gpr37l1*$^{-/-}$ pups in the absence (control) or presence of the indicated reagents, or their combinations (Shh-N: 100 nM; SANT-1:100 nM; TX14(A): 100 nM, see Materials and Methods) and plotted as percentage of BrdU-positive cells. One-way ANOVA was performed and data are shown as mean ± *SD*; $F_{(140, 11)} = 10.64$, $n = 12$, $p < 0.0001$ (*symbols indicate comparisons of WT control vs. KO samples, § WT control vs. treated WT, ° KO control vs. treated KO, + Shh-N treated WT vs. SANT-1 treated WT; significant differences identified by Bonferroni's post hoc analysis are denoted as follows: °$p < 0.05$, §§ °° $p < 0.01$, §§§$p < 0.001$, **** §§§§ ++++$p < 0.0001$). (b) Representative confocal images of Smo (red), Arl13b (green) co-immunofluorescence labeling and DAPI staining (blue) in serum-starved cerebellar primary astrocytes from *Gpr37l1*$^{+/+}$ (left) or *Gpr37l1*$^{-/-}$ (right) pups, in the absence (control) or presence of Shh-N or TX14(A) (scale bar: 10 μm). (c) Percentage of serum-starved cerebellar primary astrocytes from *Gpr37l1*$^{+/+}$ or *Gpr37l1*$^{-/-}$ pups with cilia (left) and with Smo-positive cilia (right), in the absence (control) or presence of Shh-N or TX14(A), as detected by immunofluorescence labeling of specific ciliary antigens and DAPI staining (see panel b). Left panel: no statistically significant difference was determined by one-way ANOVA followed by Bonferroni post hoc test ($F_{(42, 5)} = 1.13$, $n = 6$). Right panel: one-way ANOVA was performed and data are shown as mean ± *SD*; $F_{(66, 5)} = 25.75$, $n = 6$, $p < 0.0001$ (* symbols indicate WT control vs. KO samples, § WT control vs. treated WT, ° KO control vs. Shh-N treated KO; °° $p < 0.01$, **** §§§§$p < 0.0001$ denote significant differences identified by Bonferroni post hoc analysis) [Color figure can be viewed at wileyonlinelibrary.com]

Sofroniew, 2015) or astrocyte de-differentiation (Sirko et al., 2013) was not detected in either genotype's samples. TUNEL-positive apoptotic cells were absent in all studied experimental samples.

Arl13b-positive PC were similarly present in about 50% of Gfap-positive cells from both WT and KO cultures (Figure 2b).

RT-PCR assays (Figure 2c) on total RNA extracts from WT or KO whole brain samples and cerebellar astrocyte cultures showed the specific transcription of the *Gpr37l1* gene in all WT samples. Its closest homolog, *Gpr37*, was markedly expressed in WT whole brain samples, but scarcely transcribed in both *Gpr37l1*$^{+/+}$ and *Gpr37l1*$^{-/-}$ cultured astrocytes (Jolly et al., 2018; Yang et al., 2016). Consistently, the Gpr37 protein was absent in cerebellar primary astrocytes of both genotypes (Figure 2d).

3.3 | Genetic ablation of Gpr37l1 enhances basal and Shh-induced proliferation of cerebellar astrocyte

Specific tests were carried out to determine whether and to what extent Shh could induce cerebellar astrocytes' mitogenesis and to investigate its modulation upon ablation of Gpr37l1's function (Di Pietro et al., 2017; Marazziti et al., 2013; Ugbode et al., 2017), or treatment with the Gpr37l1-interacting, prosaposin-derived TX14(A) ligand (Liu et al., 2018; Meyer et al., 2013).

Following serum-starvation WT and KO astrocytes were cultured in the presence of varying concentrations of the biologically active N-terminal fragment of Shh (Shh-N) (Roelink et al., 1995), the Smo synthetic antagonist, SANT-1 (Chen et al., 2012) or TX14(A) and proliferation was measured by BrdU incorporation, as reported in M&M (Figures S2a and 3a). In untreated conditions, about 2%–3% of serum-starved WT cells were in proliferative state, similar to what reported for other mammalian glial cell types (Barca et al., 2007; Cragnolini et al., 2009), while Gpr37l1-deficient cultures showed on average a ca. fourfold higher basal mitotic rates.

Shh-N treatment (100 nM) induced significant increments in the percentage of proliferating WT astrocytes, while null mutant cultures did not display a significantly higher level of proliferation at all tested concentration (Figure S2a). In particular, Shh-*N* (100 nM) induced a ca. threefold increase in the percentage of proliferating WT astrocytes, compared to unstimulated cells (mean ± *SE*; WT control: 3.2 ± 0.4; KO control: 10.7 ± 0.8; WT+Shh-N: 9.4 ± 1.1; KO+Shh-N: 12.8 ± 1.1) (Figure 3a). SANT-1 (100 nM) drastically reduced the proportion of proliferating KO cells, to values comparable to those observed in WT untreated samples (mean ± *SE*; KO+SANT-1:3.8 ± 0.6) (Figure 3a).

Administration of TX14(A) at various concentrations (10–100 nM) specifically stimulated WT astrocytes, inducing mitotic levels similar to those shown by untreated KO cells, which were instead not significantly affected by TX14(A) treatment (mean ± *SE*; 100 nM TX14(A); WT TX14(A): 9.9 ± 1.3; KO TX14(A): 5.7 ± 1.1) (Figure S2a and 3a). Furthermore, the proliferative levels of WT cultures were significantly incremented upon co-treatment with Shh-*N* (100 nM), while concomitant delivering of SANT-1 (100 nM) did not significantly alter the prosaptide's effects (mean ± *SE*; TX14(A) + Shh-N; WT: 10.9 ± 1.8; TX14(A) + SANT-1:7.6 ± 1.1) (Figure 3a). One-way ANOVA with Bonferroni post hoc test was performed and data are shown as mean ± *SD* (Figure S2a: $F_{(236, 13)} = 13.99$, $n = 14$, $p < 0.0001$; Figure 3a: $F_{(140, 11)} = 10.64$, $n = 12$, $p < 0.0001$).

The levels of MAPK phosphorylation associated with cellular proliferation (Wei & Liu, 2002) were also investigated, in control conditions (Meyer et al., 2013; Okuda et al., 2016) (Figure S2b). Unstimulated KO cultures exhibited increased levels of MAPK phosphorylation, in comparison with WT cultures (**$p < 0.009$, WT vs. KO, unpaired *t* test), in agreement with the higher extent of proliferation showed by KO cells in the same experimental conditions (Figures S2 and 3a).

Thus, the constitutive absence of Gpr37l1 membrane receptor's expression upon gene ablation does increase the basal proliferation level of primary murine cerebellar astrocytes. This outcome is associated with the stimulation of the Shh–Ptch1–Smo mitogenic pathway, as it is specifically antagonized by SANT-1 treatment and accompanied by a consistent increase in MAPK phosphorylation. Interestingly, the Gpr37l1–prosaptide interaction, with consequent receptor's internalization from the plasma membrane (Meyer et al., 2013), induces a comparable, significant augment of WT astrocyte's proliferation, in the absence of any experimental treatment with exogenous Shh-N.

3.4 | Smo, Ptch1, and Gpr37l1 localize to the primary cilium in a dynamic manner

Hedgehog signaling involves binding to the transmembrane co-receptor Ptch1, relieving its inhibition of Smo, which is consequently translocated into the PC membrane. Smo, Ptch1, and Gpr37l1 membrane localization was hence analyzed by double immunofluorescence labeling. Smo was found colocalized with the PC membrane marker, Arl13b, in a small proportion of untreated WT astrocytes, but the colocalization was strikingly evident in most unstimulated KO cells (Figure 3b,c). Indeed, the percentage of ciliated cells was comparable among samples of both genotypes, in all tested conditions, while in the absence of exogenous stimuli 61.3% of KO cells had Smo localized at PC, compared to 12.5% of WT cells (Figure 3c). Shh-*N* (100 nM) treatment markedly increased the ciliary localization of Smo, in both WT and KO cells (64.9% and 88.2% of cells, respectively), while TX14(A) had a specific effect on WT astrocytes, only (56.6% of cells with Smo on cilium; Figure 3b,c). The results of one-way ANOVA with Bonferroni post hoc test are shown as mean ± *SD* (Figure 3c, left panel: $F_{(42,5)} = 1.13$, $n = 6$; right panel: $F_{(66, 5)} = 25.75$, $n = 6$, $p < 0.0001$).

Ptch1 and Gpr37l1 were found localized in correspondence of PC membranes only in unstimulated WT cultures. Addition of Shh-N or TX14(A) resulted in the absence of cilium-localized Gpr37l1 in WT samples and of cilium-localized Ptch1 (or its translocation to the ciliary base) in both WT and KO astrocytes (Figure 4).

Gpr37l1 and Ptch1 have been reported to functionally interact (Marazziti et al., 2013) and therefore their possible co-expression

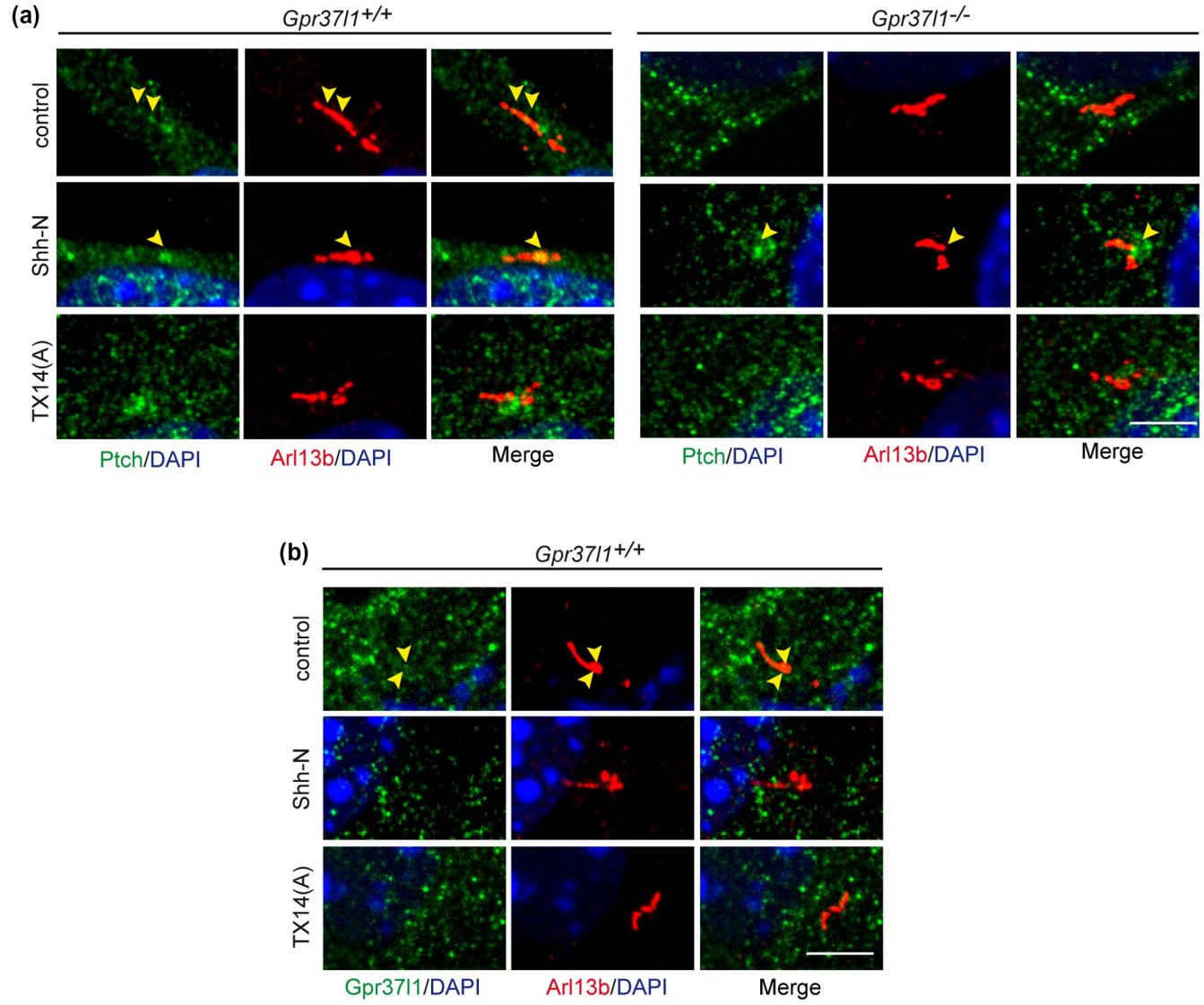

FIGURE 4 Ciliary localization of Ptch1 and Gpr37l1 in cultured cerebellar primary astrocytes. (a) Representative images of primary cilium-localized, Arl13b (red) and Ptch1 (green) immunofluorescence signals in cultured cerebellar primary astrocytes from *Gpr37l1*$^{+/+}$ or *Gpr37l1*$^{-/-}$ pups (yellow arrowheads) in the absence (control) or presence of Shh-N or TX14(A). Scale bar: 5 μm. (b) Representative images of primary cilium-localized, Arl13b (red) and Gpr37l1 (green) immunofluorescence signals in cultured cerebellar primary astrocytes from *Gpr37l1*$^{+/+}$ in the absence (control) or presence of Shh-N or TX14(A). Scale bar: 5 μm [Color figure can be viewed at wileyonlinelibrary.com]

and localization were studied in the absence or presence of Shh-N or TX14(A), by immunofluorescence labeling and Western blotting with specific antibodies.

Upon treatment with either Shh-N or TX14(A), WT astrocytes presented an increased intracellular colocalization of both Gpr37l1 and Ptch1 proteins. On the other hand, in KO cells Ptch1 always had a predominant intracellular location and aggregation, even in untreated conditions (Figure 5a).

Ptch1 protein's expression was significantly increased in KO cultures, in comparison with WT samples, while the above treatments did not significantly affect its expression levels, in cells of both genotypes (Figure 5a,c). The indicated differences were statistically significant as determined by one-way ANOVA followed by Bonferroni post hoc test. Data are shown as mean ± *SD* (Figure 5c: $F_{(29, 5)} = 9.97$, $n = 6$, $p < 0.0001$).

These findings are in agreement with the reported analysis of cerebellar samples from *Gpr37l1* KO pups (Marazziti et al., 2013) and various studies of Ptch1 localization and expression, during Shh-induced mitogenesis (Incardona et al., 2002; Yue et al., 2014). Also, Gpr37l1's expression levels in WT cultures were not altered by Shh-N or TX14(A) (Figure 5d). No statistically significant difference was determined by one-way ANOVA followed by Bonferroni post hoc test (Figure 5d: $F_{(13, 2)} = 0.13$, $n = 3$).

Cholesterol importantly affects Shh signaling cascades (Blassberg & Jacob, 2017; Mann & Beachy, 2004) and Ptch1 is involved in modulating its intracellular concentration (Bidet et al., 2011; Hu &

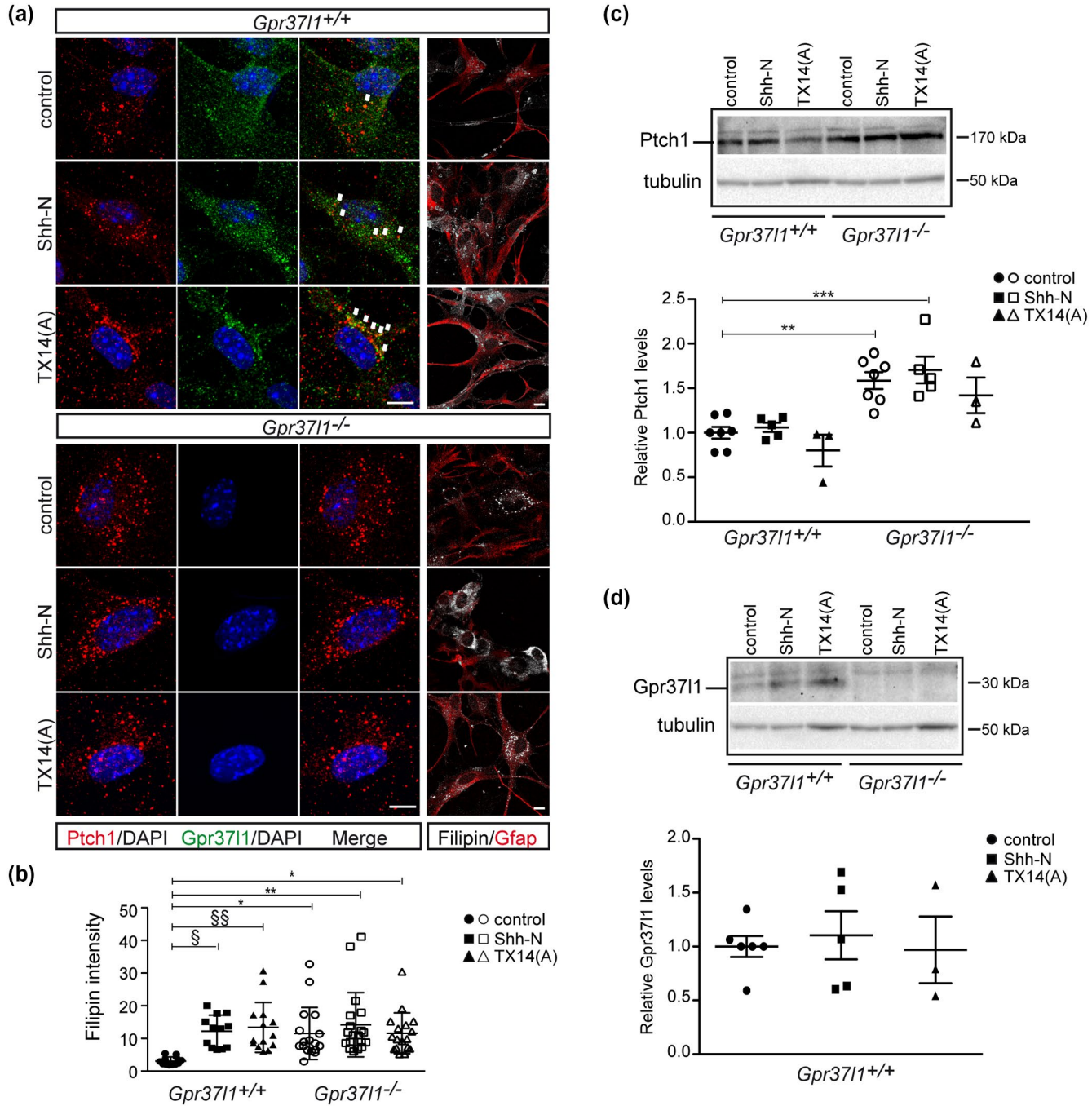

FIGURE 5 Ptch1, Gpr37l1, cholesterol localization and Ptch1, Gpr37l1 expression in cerebellar primary astrocytes from *Gpr37l1*$^{+/+}$ and *Gpr37l1*$^{-/-}$ pups, upon Shh-N or TX14(A) treatment. (a) Representative confocal images of Ptch1 (red), Gpr37l1(green) co-immunofluorescence labeling and DAPI staining (blue), or Gfap immunolabeling (red) and intracellular cholesterol staining by filipin (gray) in serum-starved cerebellar primary astrocytes from *Gpr37l1*$^{+/+}$ or *Gpr37l1*$^{-/-}$ pups, in the absence (upper panels) or presence of Shh-N or TX14(A) (lower panels). Colocalization of Ptch1 and Gpr37l1 is marked by arrows. Scale bars: 10 μm. (b) Analysis of free intracellular cholesterol staining by filipin. The indicated differences were statistically significant as determined by one-way ANOVA followed by Bonferroni post hoc test. Data are shown as mean ± *SD*; $F_{(90, 5)} = 4.01$, $n = 6$, $p < 0.003$ (* symbols indicate comparisons of WT control vs. KO samples, § WT control vs. treated WT; * §$p < 0.05$, §§ ** $p < 0.01$). (c) Representative Western blot (upper panel) and relative quantification (lower panel) of Ptch1 protein levels in cell lysates of cultured cerebellar primary astrocytes from *Gpr37l1*$^{+/+}$ or *Gpr37l1*$^{-/-}$ pups, after serum starvation followed by treatment with vehicle (control) or Shh-*N* (100 nM) or TX14(A) (100 nM). The indicated differences were statistically significant as determined by one-way ANOVA followed by Bonferroni post hoc test. Data are shown as mean ± *SD*; $F_{(29, 5)} = 9.97$, $n = 6$; $p < 0.0001$ (**$p < 0.01$, ***$p < 0.001$). (d) Representative Western blot (upper panel) and relative quantification (lower panel) of Gpr37l1 protein levels in cell lysates of cultured cerebellar primary astrocytes from *Gpr37l1*$^{+/+}$ or *Gpr37l1*$^{-/-}$ pups, after serum starvation followed by treatment with vehicle (control) or Shh-N or TX14(A). Data are shown as mean ± *SD*. No statistically significant difference was determined by one-way ANOVA followed by Bonferroni post hoc test ($F_{(13, 2)} = 0.13$, $n = 3$) [Color figure can be viewed at wileyonlinelibrary.com]

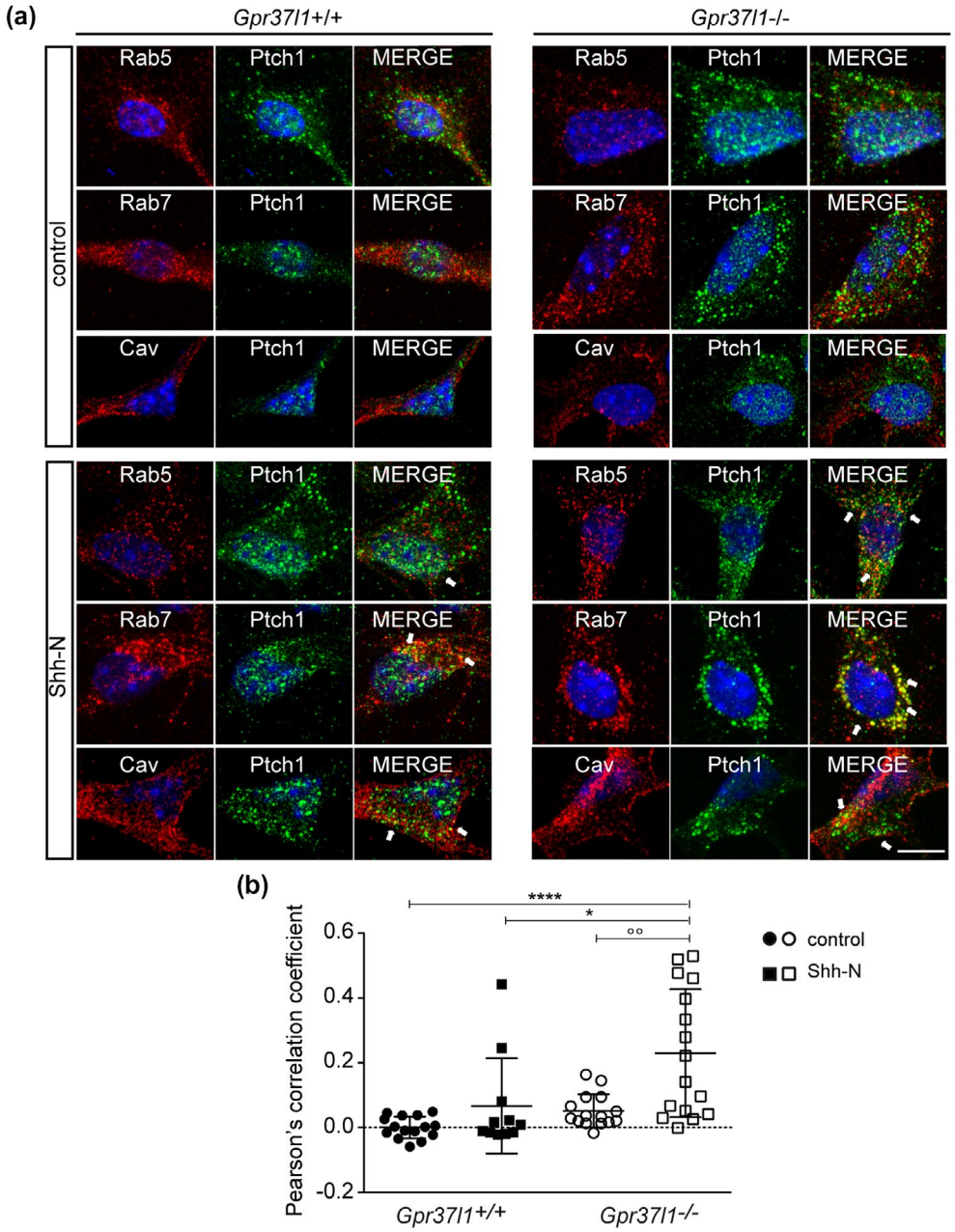

FIGURE 6 Ptch1 intracellular trafficking in cerebellar primary astrocytes from *Gpr37l1*$^{+/+}$ and *Gpr37l1*$^{-/-}$ pups, upon Shh-N treatment. (a) Representative confocal images of Ptch1 (green) and Rab5 or Rab7 (red) or caveolin 1 (Cav, red) co-immunofluorescence labeling and DAPI staining (blue) in serum-starved cerebellar primary astrocytes from *Gpr37l1*$^{+/+}$ (left) or *Gpr37l1*$^{-/-}$ (right) pups, in the absence (upper panels) or presence (lower panels) of Shh-N. Doubly positive organelles are marked by arrows. Scale bar: 10 μm. (b) The colocalization of Ptch1 and Rab7 was analyzed upon measurement of Pearson's correlation coefficient (mean ± *SE*; WT control: 0.001 ± 0.01; 0.067 ± 0.04; 0.052 ± 0.01; 0.230 ± 0.05). The indicated differences were statistically significant as determined by one-way ANOVA followed by Bonferroni post hoc test. Data are shown as mean ± *SD*; $F_{(56, 3)} = 9.52$, $n = 4$, $p < 0.0001$ (* symbols indicate comparisons of WT vs. KO samples, ° KO control vs. treated KO; * $p < 0.05$, °° $p < 0.01$, **** $p < 0.0001$) [Color figure can be viewed at wileyonlinelibrary.com]

Song, 2019). Filipin staining was performed for the analysis of free intracellular cholesterol distribution (Tabas et al., 1994) (Figure 5a). Unstimulated KO cultures showed a significantly higher extent of cholesterol, compared to untreated WT cells, consistent with the concomitant, marked increment in cilium-associated Smo (Figures 3b,c and 5a,b).

Shh-N treatment significantly increased intracellular cholesterol levels in WT cultures and comparable effects were observed upon administration of TX14(A) (Figure 5a,b; one-way ANOVA followed by Bonferroni post hoc test; data are shown as mean ± *SD*; $F_{(90, 5)} = 4.01$, $n = 6$, $p < 0.001$). These results are in accordance with studies of mitogenic Shh stimulation enhancing cellular concentration of cholesterol (Bidet et al., 2011; Hu & Song, 2019), thus critically controlling Smo enrichment at ciliary membranes and consequently intracellular signal transduction (Huang et al., 2016; Luchetti et al., 2016; Xiao et al., 2017).

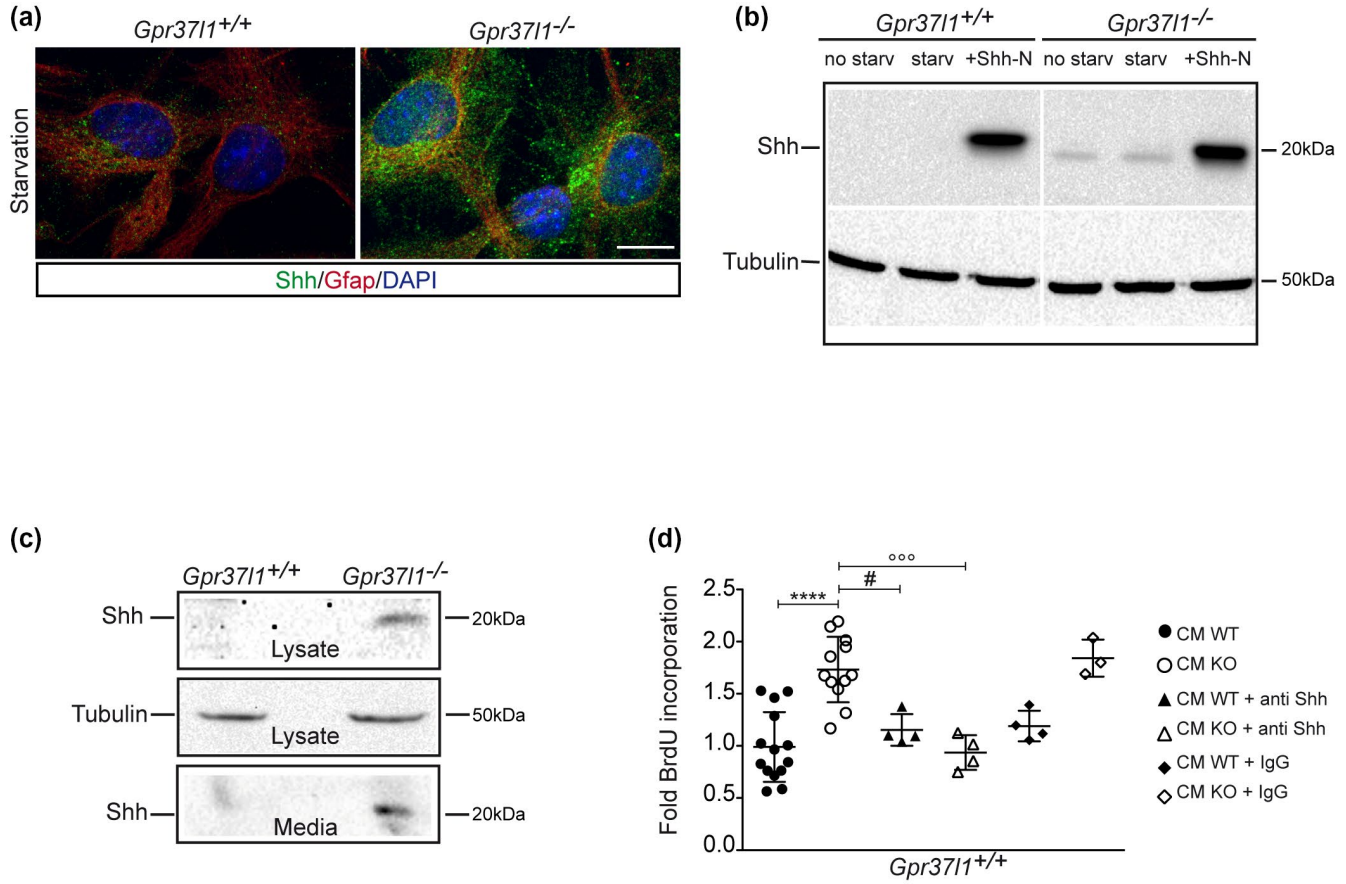

FIGURE 7 Shh localization and expression in cerebellar primary astrocytes from *Gpr37l1*$^{+/+}$ and *Gpr37l1*$^{-/-}$ pups. (a) Representative confocal images of Shh (green) and Gfap (red) co-immunofluorescence labeling and DAPI staining (blue) in serum-starved cerebellar primary astrocytes from *Gpr37l1*$^{+/+}$ or *Gpr37l1*$^{-/-}$ pups. Scale bar: 10 μm. (b) Representative Western blot of Shh protein levels in cell lysates of cerebellar primary astrocytes from *Gpr37l1*$^{+/+}$ and *Gpr37l1*$^{-/-}$ pups, in non-starved culture, or upon serum starvation and subsequent treatment with Shh-N. (c) Representative Western blot of Shh protein levels in cell lysates and media of serum-starved cerebellar primary astrocytes from *Gpr37l1*$^{+/+}$ or *Gpr37l1*$^{-/-}$ pups. (d) Quantification of BrdU incorporation in serum-starved *Gpr37l1*$^{+/+}$ cerebellar primary astrocytes grown for 24 hr in conditioned media (CM) prepared from distinct *Gpr37l1*$^{+/+}$ (WT) or *Gpr37l1*$^{-/-}$ (KO) cerebellar astrocyte cultures, in the absence (-) or presence of anti-Shh or control immunoglobulins G (IgG), and plotted as fold of stimulation compared to untreated cells. Data are shown as mean ± *SD*. The indicated differences were statistically significant as determined by one-way ANOVA followed by Bonferroni post hoc test. $F_{(40, 5)} = 12.73$; $n = 6$, $p < 0.0001$ ($^{\#}p < 0.05$, *** °°°$p < 0.0001$) [Color figure can be viewed at wileyonlinelibrary.com]

3.5 | Gpr37l1 ablation affects Shh-induced Ptch1 trafficking

Translocation of Ptch1 to intracellular endosomal/lysosomal organelles crucially regulates Smo mobilization and the activation of Shh-induced proliferative pathways (Incardona et al., 2002; Karpen et al., 2001). Membrane trafficking of Ptch1 was therefore studied in WT or KO cultures, in the absence or presence of Shh-N, upon co-labeling of caveolin 1, Rab5 or Rab7, as specific markers of plasma membrane lipid rafts, early endosomes or late endosomes, respectively (Figure 6). In untreated conditions, Ptch1 appeared to be similarly distributed with caveolin 1, Rab5, and Rab7, in both WT and KO cells. In the presence of Shh-N, Ptch1 showed a predominant intracellular distribution, in Rab7-positive, late endosomal/prelysosomal compartments (Figure 6a). The analysis of Pearson's correlation coefficient from Ptch1 and Rab7 double-immunofluorescence imaging revealed a significantly higher level of colocalization of the two proteins in KO astrocytes upon Shh-N treatment (Figure 6b; one-way ANOVA followed by Bonferroni post hoc test; data are shown as mean ± *SD*; $F_{(56, 3)} = 9.51$, $n = 4$, $p < 0.0001$).

3.6 | *Gpr37l1*$^{-/-}$ primary astrocytes produce Shh

Given the increased proliferative rate of unstimulated KO primary astrocytes, immunofluorescence staining and Western blot analysis were carried out to assess their production and secretion of active Shh. The Shh protein was markedly immunolabeled in serum-starved *Gpr37l1* null mutant samples, as well as in KO cell extracts, from both starved and not starved cultures, while control WT samples showed negligible Shh expression (Figure 7a–c).

Secreted Shh molecules were specifically detected in medium samples of KO cultures, which markedly stimulated the proliferation of distinct, testing samples of WT cells. These mitogenic effects were completely abolished in the presence of Shh-specific antibodies (Figure 7c,d; one-way ANOVA followed by Bonferroni post hoc test; data are shown as mean ± *SD*; $F_{(40, 5)} = 12.73$; $n = 6$, $p < 0.0001$).

Therefore, the genetic ablation of Gpr37l1 results in cerebellar primary astrocytes producing active Shh, which can in turn promote cellular proliferation, upon stimulation of Ptch1 intracellular translocation from the plasma membrane, intracellular cholesterol accumulation, and Smo mobilization to ciliary membrane.

4 | DISCUSSION

The production and application of validated cellular models of astroglial functions are of paramount importance in current neurobiological studies, given the fundamental role of astrocytes in inducing and regulating neuronal proliferation, differentiation, and homeostasis (Guttenplan & Liddelow, 2018; Molofsky et al., 2012). Cerebellar astrocytes, and particularly BG cells, have been the subject of intense studies because of their critical influence on pre- and postnatal differentiation and maturation of various cerebellar neuron types, including the Purkinje cells and the precursors of granule cells.

The present experimental analysis has allowed the establishment and characterization of cerebellar primary astrocyte cultures from both murine wild-type and *Gpr37l1* null mutant mouse pups, with specific expression of distinctive astrocytic markers (Hatten, 1985; Okuda et al., 2016; Pinto et al., 2000). The cultured cells are also competent for primary ciliogenesis, thus presenting a distinctive functional trait of differentiated astrocytic glia, including cerebellar BG cells, as confirmed by this study's ultrastructural investigation, as well as previous immunolabeling results and other *ex vivo* analysis of murine cerebellar tissue (Di Pietro et al., 2017; Marazziti et al., 2013; Yoshimura et al., 2011).

Shh has specific proliferative effects on mammalian glial and neural cells at embryonic, postnatal developmental stages and in adulthood (Kenney & Rowitch, 2000; Lai et al., 2003; Wechsler-Reya & Scott, 1999). The Shh–Ptch1–Smo signaling cascade also regulates the maturation and differentiation of various astrocytic cell types, including murine cerebellar BG cells, and is variably involved in modulating differentiated astroglia's functions and morphology in the adult brain (Farmer et al., 2016; Garcia et al., 2010; Hill et al., 2019). Thus, the present study has particularly focused on the analysis of the Shh–Ptch1–Smo signaling pathway, in cultured cerebellar astrocytes from mouse pups lacking the Ptch1-interacting Gpr37l1 putative membrane receptor.

Wild-type ciliated primary astrocytes respond to stimulation by Shh treatment and present increased Ptch1 internalization, intracellular cholesterol accumulation, ciliary mobilization of Smo and enhanced proliferation, as previously described in murine BG (Dahmane & Ruiz, 1999; Di Pietro et al., 2017) and other astrocytic cell types (Pitter et al., 2015; Ugbode et al., 2017; Yang et al., 2012). Under this study's culture conditions, Shh treatment did not induce morphological alterations and de-differentiation of primary astrocytes. Such reported effects may be linked to functional interactions with neuronal cells either *in vivo* or in *ex vivo* co-culturing systems (Ugbode et al., 2017; Yang et al., 2012).

Strikingly, the sole genetic ablation of the Gpr37l1 protein results in a marked increment in KO primary astrocytes basic proliferation rate, with augmented levels of Ptch1 expression and internalization, intracellular cholesterol concentration and ciliary localization of Smo. This mitogenic stimulation of *Gpr37l1*$^{-/-}$ cultures occurs in the absence of any experimental administration of exogenous Shh and it is specifically competed by the Smo antagonist, SANT-1, while presenting a concomitant robust increase in MAPK phosphorylation levels. Furthermore, the lack of the Gpr37l1 protein results in the distinctive synthesis and secretion of endogenous, mitogenically active Shh, by *Gpr37l1* null mutant astrocytes.

This study confirms previous findings regarding Gpr37l1–Ptch1 colocalization and interaction at peri-ciliary plasma membranes (Marazziti et al., 2013) and newly presents their marked co-internalization upon Shh stimulation. As those two integral membrane proteins have been shown to specifically interact, the constitutive lack of plasmalemmal Gpr37l1 in KO cultured astrocytes may favor the observed trafficking of Ptch1 to late endosomes/prelysosomes. This is clearly distinct from Ptch1 distribution in WT cultures, which presents a predominant peri-membranous localization in untreated conditions or an accumulation to early endosomes upon Shh stimulation.

The increased intracellular accumulation of Ptch1 in KO astrocytes may therefore result in a reduced extracellular efflux of cholesterol, thus provoking the reported augmentation of its intracellular levels and promoting the ciliary mobilization of Smo and other dependent mitogenic effects, in comparison with unstimulated WT control astrocytes (Bidet et al., 2011; Blassberg & Jacob, 2017; Hu & Song, 2019). Furthermore, the increased cholesterol concentration may stimulate the post-translational processing of Shh, with its lipidation and self-cleavage to the active form (Blassberg & Jacob, 2017; Chen et al., 2011; Guy, 2000).

The specific increment in cytoplasmic cholesterol concentration may conceivably stimulate the observed *de novo* production and secretion of active, endogenous Shh molecules which can thus activate and sustain the proliferation of astrocytes (Bidet et al., 2011; Hu & Song, 2019). These findings are consistent with previous reports on the synthesis and release of active Shh by mammalian astrocytes under various physiological or pathological conditions, with altered Ptch1, Smo, and cholesterol trafficking (Amankulor et al., 2009; Okuda et al., 2016; Pitter et al., 2015; Yang et al., 2012). The increased production of Shh by cerebellar astrocytes, at precocious postnatal stages, might also be involved in the observed delay of tumor occurrence and progression in a *Gpr37l1*$^{-/-}$;*Ptch1*$^{+/-}$ murine model of medulloblastoma, accelerating GCPs' exit from the proliferative state and migration to the internal granular layer (Di Pietro et al., 2019). Prosaposin, derived saposin proteins, and prosaptide analogs exert a variety of cytoprotective and stimulatory effects on different neuronal and glial cell types (Meyer et al., 2014). Saposins

and prosaptides have also been discussed as possible ligands of the Gpr37 and Gpr37l1 putative receptors, causing their internalization and activation of specific, G protein-transduced intracellular signaling cascades in primary rat astrocytes as well as some cultured cell systems (Liu et al., 2018; Lundius et al., 2014; Meyer et al., 2013, 2014). Therefore, this study has also assayed the effects of prosaptide on cerebellar primary astrocytes' proliferation and Ptch1–Smo mitogenic signaling. In the absence of Shh treatment, the administration of prosaptide TX14(A) to WT cultures markedly stimulates Gpr37l1–Ptch1 co-internalization, intracellular cholesterol accumulation and ciliary localization of Smo, as well as cell proliferation. The prosaptide-induced internalization of Gpr37l1 could thus mimics the effects of direct Shh stimulation, as it results in the co-translocation of interacting Ptch1 molecules to intracellular compartments and it may consequently stimulate astrocyte's mitogenesis. These effects can be mediated by the specific interaction of TX14(A) with the Gpr37l1 membrane receptor. In fact, the studied WT and KO primary astrocytes do not express detectable levels of the homolog Gpr37 protein while the prosaptide ligand does not significantly alters the mitogenic rate of *Gpr37l1* null mutant cultures. The co-expression of both putative receptor proteins has been shown in rat and mouse cortical primary astrocytes (Liu et al., 2018; Meyer et al., 2013). Instead, the lack of Gpr37 expression by murine cerebellar primary astrocytes reproduces a distinctive trait of astroglial differentiation in postnatal cerebellar tissue, where BG cells only express Gpr37l1 (Koirala & Corfas, 2010).

The prosaptide-induced proliferation of WT astrocytes is not markedly competed by co-treatment with the Smo antagonist, SANT-1. This could be linked to the reported activation of signal transducing $G\alpha_i$ proteins, following Gpr37l1-TX14(A) interaction (Liu et al., 2018; Meyer et al., 2013). Related mechanisms have indeed been postulated for the observed enhancement of Shh-induced mitogenesis upon peri-ciliary expression of Gpr175, another $G\alpha_i$-coupled putative receptor (Singh et al., 2015). It should also be noted that both Gpr37l1 and prosaposin are specifically expressed in human gliomas and glioblastomas, with prosaposin actively promoting cell proliferation and tumorigenesis (Jiang et al., 2018, 2019; Wu et al., 2019).

Further studies will therefore be necessary to comprehensively assess the activation and regulation of mitogenesis in cerebellar astrocytes upon stimulation of Gpr37l1 and related GPRs by cognate natural or synthetic ligands, in different physiological or pathological systems. The indication of prosaposin and prosaptides as specific ligands has been debated and it will thus be interesting to further investigate whether the plasma membrane co-expression of Gpr37l1 and Ptch1 may actually be required for activating ligand–receptor interaction and intracellular signal transduction. The experimental expression of Gpr37l1 and Ptch1 in cultured KO astrocytes will also allow to specifically test the rescue of phenotypes described in this study. Moreover, the availability of appropriate *ex vivo* culture systems will be instrumental in setting up the detailed biochemical and physiological analysis of molecular mechanisms that induce and modulate production and secretion of Shh and related hormones by cerebellar astrocytes, as well as the specific regulatory and stimulatory effects exerted by saposins and derived cytoprotective factors.

DECLARATION OF TRANSPARENCY

The authors, reviewers and editors affirm that in accordance to the policies set by the *Journal of Neuroscience Research*, this manuscript presents an accurate and transparent account of the study being reported and that all critical details describing the methods and results are present.

ACKNOWLEDGMENTS

The authors greatly thank Emerald Perlas for revising the manuscript; M. Valenza for advice on filipin staining; G. D' Erasmo and A. Ventrera for excellent technical assistance; and F. Ferrara and T. Cuccurullo for secretarial assistance.

CONFLICT OF INTEREST

The authors declare no conflict of interest.

AUTHOR CONTRIBUTIONS

All authors had full access to all the data in the study and take responsibility for the integrity of the data and the accuracy of the data analysis. *Conceptualization*, G.L.S., C.D.P., R.M., and D.M.; *Methodology*, G.L.S., C.D.P., and G.B.; *Investigation*, G.L.S., C.D.P., and G.B.; *Formal Analysis*, G.L.S., C.D.P., R.M., and DM.; *Writing – Original Draft*, D.M. and R.M.; *Writing – Review & Editing*, D.M., R.M., G.L.S., C.D.P., G.B., and G.T.V.; *Funding Acquisition*, G.T.V.

PEER REVIEW

The peer review history for this article is available at https://publons.com/publon/10.1002/jnr.24775.

DATA AVAILABILITY STATEMENT

The data that support the findings of this study are openly available in Open Science Framework at http://doi.org/10.17605/OSF.IO/97AP2, RRID:SCR_003238).

ORCID

Daniela Marazziti https://orcid.org/0000-0002-1582-9271

REFERENCES

Allen, B. L., Song, J. Y., Izzi, L., Althaus, I. W., Kang, J.-S., Charron, F., Krauss, R. S., & McMahon, A. P. (2011). Overlapping roles and collective requirement for the coreceptors GAS1, CDO, and BOC in SHH pathway function. *Developmental Cell*, *20*(6), 775–787. https://doi.org/10.1016/j.devcel.2011.04.018

Amankulor, N. M., Hambardzumyan, D., Pyonteck, S. M., Becher, O. J., Joyce, J. A., & Holland, E. C. (2009). Sonic hedgehog pathway activation is induced by acute brain injury and regulated by injury-related inflammation. *Journal of Neuroscience*, *29*(33), 10299–10308. https://doi.org/10.1523/JNEUROSCI.2500-09.2009

Barca, O., Seoane, M., Ferré, S., Prieto, J. M., Lema, M., Señarís, R., & Arce, V. M. (2007). Mechanisms of interferon-β-induced survival

in fetal and neonatal primary astrocytes. *NeuroImmunomodulation*, *14*(1), 39–45. https://doi.org/10.1159/000107287

Berbari, N. F., Bishop, G. A., Askwith, C. C., Lewis, J. S., & Mykytyn, K. (2007). Hippocampal neurons possess primary cilia in culture. *Journal of Neuroscience Research*, *85*(5), 1095–1100. https://doi.org/10.1002/jnr.21209

Bidet, M., Joubert, O., Lacombe, B., Ciantar, M., Nehmé, R., Mollat, P., Brétillon, L., Faure, H., Bittman, R., Ruat, M., & Mus-Veteau, I. (2011). The hedgehog receptor patched is involved in cholesterol transport. *PLoS ONE*, *6*(9), 1–11. https://doi.org/10.1371/journal.pone.0023834

Bishop, G. A., Berbari, N. F., Lewis, J., & Mykytyn, K. (2007). Type III adenylyl cyclase localizes to primary cilia throughout the adult mouse brain. *Journal of Comparative Neurology*, *505*(5), 562–571. https://doi.org/10.1002/cne.21510

Blassberg, R., & Jacob, J. (2017). Lipid metabolism fattens up hedgehog signaling. *BMC Biology*, *15*, 1–14. https://doi.org/10.1186/s12915-017-0442-y

Buffo, A., & Rossi, F. (2013). Origin, lineage and function of cerebellar glia. *Progress in Neurobiology*, *109*, 42–63. https://doi.org/10.1016/j.pneurobio.2013.08.001

Buosi, A. S., Matias, I., Araujo, A. P. B., Batista, C., & Gomes, F. C. A. (2018). Heterogeneity in synaptogenic profile of astrocytes from different brain regions. *Molecular Neurobiology*, *55*, 751–762. https://doi.org/10.1007/s12035-016-0343-z

Chen, M., Huang, J., Yang, X., Liu, B., Zhang, W., Huang, L. I., Deng, F., Ma, J., Bai, Y., Lu, R., Huang, B., Gao, Q., Zhuo, Y., & Ge, J. (2012). Serum starvation induced cell cycle synchronization facilitates human somatic cells reprogramming. *PLoS ONE*, *7*(4), e28203. https://doi.org/10.1371/journal.pone.0028203

Chen, X., Tukachinsky, H., Huang, C.-H., Jao, C., Chu, Y.-R., Tang, H.-Y., Mueller, B., Schulman, S., Rapoport, T. A., & Salic, A. (2011). Processing and turnover of the Hedgehog protein in the endoplasmic reticulum. *Journal of Cell Biology*, *192*(5), 825–838. https://doi.org/10.1083/jcb.201008090

Chizhikov, V. V., Davenport, J., Zhang, Q., Shih, E. K., Cabello, O. A., Fuchs, J. L., Yoder, B. K., & Millen, K. J. (2007). Cilia proteins control cerebellar morphogenesis by promoting expansion of the granule progenitor pool. *Journal of Neuroscience*, *27*(36), 9780–9789. https://doi.org/10.1523/JNEUROSCI.5586-06.2007

Cragnolini, A. B., Huang, Y., Gokina, P., & Friedman, W. J. (2009). Nerve growth factor attenuates proliferation of astrocytes via the p75 neurotrophin receptor. *Glia*, *57*(13), 1386–1392. https://doi.org/10.1002/glia.20857

Dahmane, N., & Ruiz, A. (1999). Sonic hedgehog and cerebellum development. *Development*, *3100*, 3089–3100.

De Luca, A., Cerrato, V., Fucà, E., Parmigiani, E., Buffo, A., & Leto, K. (2016). Sonic hedgehog patterning during cerebellar development. *Cellular and Molecular Life Sciences*, *73*(2), 291–303. https://doi.org/10.1007/s00018-015-2065-1

Di Pietro, C., La Sala, G., Matteoni, R., Marazziti, D., & Tocchini-Valentini, G. P. (2019). Genetic ablation of Gpr37l1 delays tumor occurrence in Ptch1 +/− mouse models of medulloblastoma. *Experimental Neurology*, *312*, 33–42. https://doi.org/10.1016/j.expneurol.2018.11.004

Di Pietro, C., Marazziti, D., La Sala, G., Abbaszadeh, Z., Golini, E., Matteoni, R., & Tocchini-Valentini, G. P. (2017). Primary cilia in the murine cerebellum and in mutant models of medulloblastoma. *Cellular and Molecular Neurobiology*, *37*(1), 145–154. https://doi.org/10.1007/s10571-016-0354-3

Doetsch, F., Garcìa-Verdugo, J. M., & Alvarez-Buylla, A. (1997). Cellular composition and three-dimensional organization of thesubventricular germinal zone in the adult mammalian brain. *Journal of Neuroscience*, *17*(13), 5046–5061. https://doi.org/10.1523/JNEUROSCI.17-13-05046.1997

Eddleston, M., & Mucke, L. (1993). Molecular profile of reactive astrocytes—Implications for their role in neurologic disease. *Neuroscience*, *54*(1), 15–36. https://doi.org/10.1016/0306-4522(93)90380-X

Farmer, W. T., Abrahamsson, T., Chierzi, S., Lui, C., Zaelzer, C., Jones, E. V., Bally, B. P., Chen, G. G., Theroux, J.-F., Peng, J., Bourque, C. W., Charron, F., Ernst, C., Sjostrom, P. J., & Murai, K. K. (2016). Neurons diversify astrocytes in the adult brain through sonic hedgehog signaling. *Science*, *351*(6275), 849–854. https://doi.org/10.1126/science.aab3103

Farmer, W. T., & Murai, K. (2017). Resolving astrocyte heterogeneity in the CNS. *Frontiers in Cellular Neuroscience*, *11*, e00300. https://doi.org/10.3389/fncel.2017.00300

Garcia, A. D. R., Petrova, R., Eng, L., & Joyner, A. L. (2010). Sonic Hedgehog regulates discrete populations of astrocytes in the adult mouse forebrain. *Journal of Neuroscience*, *30*(41), 13597–13608. https://doi.org/10.1523/JNEUROSCI.0830-10.2010

Gerdes, J. M., Liu, Y., Zaghloul, N. A., Leitch, C. C., Lawson, S. S., Kato, M., Beachy, P. A., Beales, P. L., DeMartino, G. N., Fisher, S., Badano, J. L., & Katsanis, N. (2007). Disruption of the basal body compromises proteasomal function and perturbs intracellular Wnt response. *Nature Genetics*, *39*(11), 1350–1360. https://doi.org/10.1038/ng.2007.12

Guttenplan, K. A., & Liddelow, S. A. (2018). Astrocytes and microglia: Models and tools. *Journal of Experimental Medicine*, *216*(1), 71–83. https://doi.org/10.1084/jem.20180200

Guy, R. K. (2000). Inhibition of sonic hedgehog autoprocessing in cultured mammalian cells by sterol deprivation. *Proceedings of the National Academy of Sciences of the United States of America*, *97*(13), 7307–7312. https://doi.org/10.1073/pnas.97.13.7307

Han, Y. G., Spassky, N., Romaguera-Ros, M., Garcia-Verdugo, J. M., Aguilar, A., Schneider-Maunoury, S., & Alvarez-Buylla, A. (2008). Hedgehog signaling and primary cilia are required for the formation of adult neural stem cells. *Nature Neuroscience*, *11*(3), 277–284. https://doi.org/10.1038/nn2059

Hatten, M. E. (1985). Neuronal regulation of astroglial morphology and proliferation in vitro. *Journal of Cell Biology*, *100*(2), 384–396. https://doi.org/10.1083/jcb.100.2.384

Hill, S. A., Blaeser, A. S., Coley, A. A., Xie, Y., Shepard, K. A., Harwell, C. C., Gao, W.-J., & Garcia, A. D. R. (2019). Sonic hedgehog signaling in astrocytes mediates cell type-specific synaptic organization. *eLife*, *8*, 1–23. https://doi.org/10.7554/eLife.45545

Ho, K. S., & Scott, M. P. (2002). Sonic hedgehog in the nervous system: Functions, modifications and mechanisms. *Current Opinion in Neurobiology*, *12*(1), 57–63. https://doi.org/10.1016/S0959-4388(02)00290-8

Hrabě de Angelis, M., Nicholson, G., Selloum, M., White, J. K., Morgan, H., Ramirez-Solis, R., Sorg, T., Wells, S., Fuchs, H., Fray, M., Adams, D. J., Adams, N. C., Adler, T., Aguilar-Pimentel, A., Ali-Hadji, D., Amann, G., André, P., Atkins, S., Auburtin, A., … Brown, S. D. M. (2015). Analysis of mammalian gene function through broad-based phenotypic screens across a consortium of mouse clinics. *Nature Genetics*, *47*(9), 969–978. https://doi.org/10.1038/ng.3360

Hu, A., & Song, B. L. (2019). The interplay of Patched, Smoothened and cholesterol in Hedgehog signaling. *Current Opinion in Cell Biology*, *61*, 31–38. https://doi.org/10.1016/j.ceb.2019.06.008

Hu, X., Qin, S., Huang, X., Yuan, Y., Tan, Z., Gu, Y., Cheng, X., Wang, D., Lian, X.-F., He, C., & Su, Z. (2019). Region-restrict astrocytes exhibit heterogeneous susceptibility to neuronal reprogramming. *Stem Cell Reports*, *12*(2), 290–304. https://doi.org/10.1016/j.stemcr.2018.12.017

Huang, P., Nedelcu, D., Watanabe, M., Jao, C., Kim, Y., Liu, J., & Salic, A. (2016). Cellular cholesterol directly activates smoothened in hedgehog signaling. *Cell*, *166*, 1176–1187. https://doi.org/10.1016/j.cell.2016.08.003

Incardona, J. P., Gruenberg, J., & Roelink, H. (2002). Sonic hedgehog induces the segregation of patched and smoothened in endosomes.

Current Biology, *12*, 983–995. https://doi.org/10.1016/S0960-9822(02)00895-3

Izzi, L., Lévesque, M., Morin, S., Laniel, D., Wilkes, B. C., Mille, F., Krauss, R. S., McMahon, A. P., Allen, B. L., & Charron, F. (2011). Boc and gas1 each form distinct shh receptor complexes with ptch1 and are required for shh-mediated cell proliferation. *Developmental Cell*, *20*(6), 788–801. https://doi.org/10.1016/j.devcel.2011.04.017

Jiang, Y., Zhou, J., Hou, D., Luo, P., Gao, H., Ma, Y., & Li, L. (2019). Prosaposin is a biomarker of mesenchymal glioblastoma and regulates mesenchymal transition through the TGF-β1/Smad signaling pathway. *Journal of Pathology*, *249*, 26–38. https://doi.org/10.1002/path.5278

Jiang, Y., Zhou, J., Luo, P., Gao, H., Ma, Y., Chen, Y.-S., Li, L., Zou, D., Zhang, Y. E., & Jing, Z. (2018). Prosaposin promotes the proliferation and tumorigenesis of glioma through toll-like receptor 4 (TLR4)-mediated NF-κB signaling pathway. *EBioMedicine*, *37*, 78–90. https://doi.org/10.1016/j.ebiom.2018.10.053

Jolly, S., Bazargani, N., Quiroga, A. C., Pringle, N. P., Attwell, D., Richardson, W. D., & Li, H. (2018). G protein-coupled receptor 37-like 1 modulates astrocyte glutamate transporters and neuronal NMDA receptors and is neuroprotective in ischemia. *Glia*, *66*(1), 47–61. https://doi.org/10.1002/glia.23198

Karpen, H. E., Bukowski, J. T., Hughes, T., Gratton, J. P., Sessa, W. C., & Gailani, M. R. (2001). The sonic hedgehog receptor patched associates with caveolin-1 in cholesterol-rich microdomains of the plasma membrane. *Journal of Biological Chemistry*, *276*(22), 19503–19511. https://doi.org/10.1074/jbc.M010832200

Kenney, A. M., & Rowitch, D. H. (2000). Sonic hedgehog promotes G1 cyclin expression and sustained cell cycle progression in mammalian neuronal precursors. *Molecular and Cellular Biology*, *20*(23), 9055–9067. https://doi.org/10.1128/mcb.20.23.9055-9067.2000

Kiprilov, E. N., Awan, A., Desprat, R., Velho, M., Clement, C. A., Byskov, A. G., Andersen, C. Y., Satir, P., Bouhassira, E. E., Christensen, S. T., & Hirsch, R. E. (2008). Human embryonic stem cells in culture possess primary cilia with hedgehog signaling machinery. *Journal of Cell Biology*, *180*(5), 897–904. https://doi.org/10.1083/jcb.200706028

Koirala, S., & Corfas, G. (2010). Identification of novel glial genes by single-cell transcriptional profiling of Bergmann glial cells from mouse cerebellum. *PLoS ONE*, *5*(2), e9198. https://doi.org/10.1371/journal.pone.0009198

Lai, K., Kaspar, B. K., Gage, F. H., & Schaffer, D. V. (2003). Sonic hedgehog regulates adult neural progenitor proliferation in vitro and in vivo. *Nature Neuroscience*, *6*, 21–27. https://doi.org/10.1038/nn983

Leto, K., Arancillo, M., Becker, E. B. E., Buffo, A., Chiang, C., Ding, B., Dobyns, W. B., Dusart, I., Haldipur, P., Hatten, M. E., Hoshino, M., Joyner, A. L., Kano, M., Kilpatrick, D. L., Koibuchi, N., Marino, S., Martinez, S., Millen, K. J., Millner, T. O., … Hawkes, R. (2016). Consensus paper: Cerebellar development. *Cerebellum*, *15*, 789–828. https://doi.org/10.1007/s12311-015-0724-2

Liu, B., Mosienko, V., Vaccari Cardoso, B., Prokudina, D., Huentelman, M., Teschemacher, A. G., & Kasparov, S. (2018). Glio- and neuro-protection by prosaposin is mediated by orphan G-protein coupled receptors GPR37L1 and GPR37. *Glia*, *66*(11), 2414–2426. https://doi.org/10.1002/glia.23480

Liu, B., Teschemacher, A. G., & Kasparov, S. (2017). Astroglia as a cellular target for neuroprotection and treatment of neuro-psychiatric disorders. *Glia*, *65*(8), 1205–1226. https://doi.org/10.1002/glia.23136

Luchetti, G., Sircar, R., Kong, J. H., Nachtergaele, S., Sagner, A., Byrne, E. F. X., Covey, D. F., Siebold, C., & Rohatgi, R. (2016). Cholesterol activates the G-protein coupled receptor Smoothened to promote Hedgehog signaling. *eLife*, *5*, e20304. https://doi.org/10.7554/eLife.20304

Lundius, E. G., Vukojević, V., Hertz, E., Stroth, N., Cederlund, A., Hiraiwa, M., Terenius, L., & Svenningsson, P. (2014). GPR37 protein trafficking to the plasma membrane regulated by prosaposin and GM1 gangliosides promotes cell viability. *Journal of Biological Chemistry*, *289*(8), 4660–4673. https://doi.org/10.1074/jbc.M113.510883

Mann, R. K., & Beachy, P. A. (2004). Novel lipid modifications of secreted protein signals. *Annual Review of Biochemistry*, *73*(1), 891–923. https://doi.org/10.1146/annurev.biochem.73.011303.073933

Marazziti, D., Di Pietro, C., Golini, E., Mandillo, S., La Sala, G., Matteoni, R., & Tocchini-Valentini, G. P. (2013). Precocious cerebellum development and improved motor functions in mice lacking the astrocyte cilium-, patched 1-associated Gpr37l1 receptor. *Proceedings of the National Academy of Sciences of the United States of America*, *110*(41), 16486–16491. https://doi.org/10.1073/pnas.1314819110

Marazziti, D., Gallo, A., Golini, E., Matteoni, R., & Tocchini-Valentini, G. P. (1998). Molecular cloning and chromosomal localization of the mouse Gpr37 gene encoding an orphan G-protein-coupled peptide receptor expressed in brain and testis. *Genomics*, *53*(3), 315–324. https://doi.org/10.1006/geno.1998.5433

Marazziti, D., Golini, E., Gallo, A., Lombardi, M. S., Matteoni, R., & Tocchini-Valentini, G. P. (1997). Cloning of GPR37, a gene located on chromosome 7 encoding a putative g- protein-coupled peptide receptor, from a human frontal brain EST library. *Genomics*, *45*(1), 68–77. https://doi.org/10.1006/geno.1997.4900

Marazziti, D., Golini, E., Mandillo, S., Magrelli, A., Witke, W., Matteoni, R., & Tocchini-Valentini, G. P. (2004). Altered dopamine signaling and MPTP resistance in mice lacking the Parkinson's disease-associated GPR37/parkin-associated endothelin-like receptor. *Proceedings of the National Academy of Sciences of the United States of America*, *101*(27), 10189–10194. https://doi.org/10.1073/pnas.0403661101

Mason, C. A. (1988). The extending astroglial process: Development of glial cell shape, the growing tip, and interactions with neurons. *Journal of Neuroscience*, *8*, 3124–3134.

Matyash, V., & Kettenmann, H. (2010). Heterogeneity in astrocyte morphology and physiology. *Brain Research Reviews*, *63*(1–2), 2–10. https://doi.org/10.1016/j.brainresrev.2009.12.001

Meehan, T. F., Conte, N., West, D. B., Jacobsen, J. O., Mason, J., Warren, J., Chen, C.-K., Tudose, I., Relac, M., Matthews, P., Karp, N., Santos, L., Fiegel, T., Ring, N., Westerberg, H., Greenaway, S., Sneddon, D., Morgan, H., Codner, G. F., … Smedley, D. (2017). Disease model discovery from 3,328 gene knockouts by the International Mouse Phenotyping Consortium. *Nature Genetics*, *49*(8), 1231–1238. https://doi.org/10.1038/ng.3901

Meyer, R. C., Giddens, M. M., Coleman, B. M., & Hall, R. A. (2014). The protective role of prosaposin and its receptors in the nervous system. *Brain Research*, *1585*, 1–12. https://doi.org/10.1016/j.brainres.2014.08.022

Meyer, R. C., Giddens, M. M., Schaefer, S. A., & Hall, R. A. (2013). GPR37 and GPR37L1 are receptors for the neuroprotective and glioprotective factors prosaptide and prosaposin. *Proceedings of the National Academy of Sciences of the United States of America*, *110*(23), 9529–9534. https://doi.org/10.1073/pnas.1219004110

Molofsky, A. V., Krenick, R., Ullian, E., Tsai, H., Deneen, B., Richardson, W. D., & Rowitch, D. H. (2012). Astrocytes and disease: A neurodevelopmental perspective. *Genes and Development*, *26*(9), 891–907. https://doi.org/10.1101/gad.188326.112.tal

Muller, C. P., Stephany, D. A., Winkler, D. F., Hoeg, J. M., Demosky, S. J., & Wunderlich, J. R. (1984). Filipin as a flow microfluorometry probe for cellular cholesterol. *Citometry*, *5*, 42–54. https://doi.org/10.1002/cyto.990050108

Okuda, H. (2018). A review of functional heterogeneity among astrocytes and the CS56-specific antibody-mediated detection of a subpopulation of astrocytes in adult brains. *Anatomical Science International*, *93*(2), 161–168. https://doi.org/10.1007/s12565-017-0420-z

Okuda, H., Tatsumi, K., Morita-Takemura, S., Nakahara, K., Nochioka, K., Shinjo, T., Terada, Y., & Wanaka, A. (2016). Hedgehog signaling modulates the release of gliotransmitters from cultured cerebellar astrocytes. *Neurochemical Research*, *41*(1–2), 278–289. https://doi.org/10.1007/s11064-015-1791-y

Ott, C., & Lippincott-Schwartz, J. (2012). Visualization of live primary cilia dynamics using fluorescence microscopy. *Current Protocols in Cell Biology*, *57*, 1–22. https://doi.org/10.1002/0471143030.cb0426s57

Palay, S. L., & Chan-Palay, V. (1974). *Cerebellar cortex*. Springer. https://doi.org/10.1007/978-3-642-65581-4

Pedersen, L. B., Mogensen, J. B., & Christensen, S. T. (2016). Endocytic control of cellular signaling at the primary cilium. *Trends in Biochemical Sciences*, *41*(9), 784–797. https://doi.org/10.1016/j.tibs.2016.06.002

Pinto, S. S., Gottfried, C., Mendez, A., Gonçalves, D., Karl, J., Gonçalves, C. A., Wofchuk, S., & Rodnight, R. (2000). Immunocontent and secretion of S100B in astrocyte cultures from different brain regions in relation to morphology. *FEBS Letters*, *486*(3), 203–207. https://doi.org/10.1016/S0014-5793(00)02301-2

Pitter, K. L., Tamagno, I., Feng, X., Ghosal, K., & Amankulor, N. (2015). HHS public access. *Glia*, *62*(10), 1595–1607. https://doi.org/10.1002/glia.22702

Roelink, H., Porter, J. A., Chiang, C., Tanabe, Y., Chang, D. T., Beachy, P. A., & Jessell, T. M. (1995). Floor plate and motor neuron induction by different concentrations of the amino-terminal cleavage product of sonic hedgehog autoproteolysis. *Cell*, *81*, 445–455. https://doi.org/10.1016/0092-8674(95)90397-6

Singh, J., Wen, X., & Scales, S. J. (2015). The orphan G protein-coupled receptor Gpr175 (Tpra40) enhances Hedgehog signaling by modulating cAMP levels. *Journal of Biological Chemistry*, *290*(49), 29663–29675. https://doi.org/10.1074/jbc.M115.665810

Singla, V., & Reiter, J. F. (2006). The primary cilium as the cell's antenna: Signaling at a sensory organelle. *Science*, *313*(5787), 629–633. https://doi.org/10.1126/science.1124534

Sirko, S., Behrendt, G., Johansson, P. A., Tripathi, P., Costa, M. R., Bek, S., Heinrich, C., Tiedt, S., Colak, D., Dichgans, M., Fischer, I. R., Plesnila, N., Staufenbiel, M., Haass, C., Snapyan, M., Saghatelyan, A., Tsai, L.-H., Fischer, A., Grobe, K., … Götz, M. (2013). Reactive glia in the injured brain acquire stem cell properties in response to sonic hedgehog. *Cell Stem Cell*, *12*(4), 426–439. https://doi.org/10.1016/j.stem.2013.01.019

Smith, N. J. (2015). Drug discovery opportunities at the endothelin B receptor-related orphan G protein-coupled receptors, GPR37 and GPR37L1. *Frontiers in Pharmacology*, *6*, 1–13. https://doi.org/10.3389/fphar.2015.00275

Sofroniew, M. V. (2015). Astrogliosis. *Cold Spring Harbor Perspective in Biology*, *7*, a020420. https://doi.org/10.1101/cshperspect.a020420

Spassky, N., Han, Y.-G., Aguilar, A., Strehl, L., Besse, L., Laclef, C., Romaguera Ros, M., Garcia-Verdugo, J. M., & Alvarez-Buylla, A. (2008). Primary cilia are required for cerebellar development and Shh-dependent expansion of progenitor pool. *Developmental Biology*, *317*(1), 246–259. https://doi.org/10.1016/j.ydbio.2008.02.026

Tabas, I., Zha, X., Beatini, N., Myers, J. N., & Maxfield, F. R. (1994). The actin cytoskeleton is important for the stimulation of cholesterol esterification by atherogenic lipoproteins in macrophages. *Journal of Biological Chemistry*, *269*(36), 22547–22556.

Traiffort, E., Charytoniuk, D. A., Faure, H., & Ruat, M. (2002). Regional distribution of sonic hedgehog, patched, and smoothened mRNA in the adult rat brain. *Journal of Neurochemistry*, *70*(3), 1327–1330. https://doi.org/10.1046/j.1471-4159.1998.70031327.x

Ugbode, C. I., Smith, I., Whalley, B. J., Hirst, W. D., & Rattray, M. (2017). Sonic hedgehog signalling mediates astrocyte crosstalk with neurons to confer neuroprotection. *Journal of Neurochemistry*, *142*(3), 429–443. https://doi.org/10.1111/jnc.14064

Valdenaire, O., Giller, T., Breu, V., Ardati, A., Schweizer, A., & Richards, J. G. (1998). A new family of orphan G protein-coupled receptors predominantly expressed in the brain. *FEBS Letters*, *424*(3), 193–196. https://doi.org/10.1016/S0014-5793(98)00170-7

Wallace, V. A., & Raff, M. C. (1999). A role for Sonic hedgehog in axon-to-astrocyte signalling in the rodent optic nerve. *Development*, *126*(13), 2901–2909.

Wechsler-Reya, R. J., & Scott, M. P. (1999). Control of neuronal precursor proliferation in the cerebellum by sonic hedgehog. *Neuron*, *22*(1), 103–114. https://doi.org/10.1016/S0896-6273(00)80682-0

Wei, Z., & Liu, H. T. (2002). MAPK signal pathways in the regulation of cell proliferation in mammalian cells. *Cell Research*, *12*(1), 9–18. https://doi.org/10.1038/sj.cr.7290105

Wu, V., Yeerna, H., Nohata, X. N., Chiou, X. J., Harismendy, X. O., Raimondi, F., & Gutkind, J. S. (2019). Illuminating the Onco-GPCRome: Novel G protein—Coupled receptor-driven oncocrine networks and targets for cancer immunotherapy. *Journal of Biological Chemistry*, *294*(29), 11062–11086. https://doi.org/10.1074/jbc.REV119.005601

Xiao, X. U., Tang, J.-J., Peng, C., Wang, Y., Fu, L., Qiu, Z.-P., Xiong, Y., Yang, L.-F., Cui, H.-W., He, X.-L., Yin, L., Qi, W., Wong, C. C. L., Zhao, Y., Li, B.-L., Qiu, W.-W., & Song, B.-L. (2017). Cholesterol modification of smoothened is required for hedgehog signaling. *Molecular Cell*, *66*(1), 154–162.e10. https://doi.org/10.1016/j.molcel.2017.02.015

Yang, H., Feng, G., Olivera, C., Jiao, X., Vitale, A., Gong, J., & You, S. (2012). Sonic hedgehog released from scratch-injured astrocytes is a key signal necessary but not sufficient for the astrocyte de-differentiation. *Stem Cell Research*, *9*(2), 156–166. https://doi.org/10.1016/j.scr.2012.06.002

Yang, H. J., Vainshtein, A., Maik-Rachline, G., & Peles, E. (2016). G protein-coupled receptor 37 is a negative regulator of oligodendrocyte differentiation and myelination. *Nature Communications*, *7*, 1–11. https://doi.org/10.1038/ncomms10884

Yoshimura, K., Kawate, T., & Takeda, S. (2011). Signaling through the primary cilium affects glial cell survival under a stressed environment. *Glia*, *59*(2), 333–344. https://doi.org/10.1002/glia.21105

Yue, S., Tang, L.-Y., Tang, Y., Tang, Y. I., Shen, Q.-H., Ding, J., Chen, Y., Zhang, Z., Yu, T.-T., Zhang, Y. E., & Cheng, S. Y. (2014). Requirement of Smurf-mediated endocytosis of Patched1 in sonic hedgehog signal reception. *eLife*, *3*, 1–24. https://doi.org/10.7554/eLife.02555

Zhang, J., Lipinski, R. J., Gipp, J. J., Shaw, A. K., & Bushman, W. (2009). Hedgehog pathway responsiveness correlates with the presence of primary cilia on prostate stromal cells. *BMC Developmental Biology*, *9*(1), 1–7. https://doi.org/10.1186/1471-213X-9-50

SUPPORTING INFORMATION

Additional Supporting Information may be found online in the Supporting Information section.

Supplementary Material

FIGURE S1 Immunocytochemical characterization of cultured cerebellar primary astrocytes. (a) Representative images of Glast immunofluorescence labeling (green) and DAPI staining (blue) in serum-starved cultured cerebellar astrocytes from *Gpr37l1*$^{+/+}$ or *Gpr37l1*$^{-/-}$ pups. Scale bar: 10 μm. (b) Representative images of Aqp4 immunofluorescence labeling (red) and DAPI staining (blue) in serum-starved cultured cerebellar astrocytes from *Gpr37l1*$^{+/+}$ or *Gpr37l1*$^{-/-}$ pups. Scale bar: 20 μm. (c) Representative confocal images of Olig2, Cntn2 or Iba1 (green) and Gfap (red) co-immunofluorescence labeling and DAPI staining (blue) in serum-starved cultured cerebellar astrocytes from *Gpr37l1*$^{+/+}$ pups. Scale bar: 20 μm. (d) Representative images of different forms of astrocytic glia cells, as detected in cultured cerebellar astrocytes from *Gpr37l1*$^{+/+}$ or *Gpr37l1*$^{-/-}$ pups by Gfap immunofluorescence labelling (red). Scale bar: 50 μm

FIGURE S2 Reagent's concentration effects on Shh-N- and TX14(A)-induced proliferation in cultured primary astrocytes from *Gpr37l1*$^{+/+}$ and *Gpr37l1*$^{-/-}$ pups. (a) BrdU incorporation was quantified in

cerebellar primary astrocytes from *Gpr37l1*$^{+/+}$ or *Gpr37l1*$^{-/-}$ pups in absence (control, 0 nM) or presence of increasing concentrations of Shh-N or TX14(A) and plotted as percentage of BrdU-positive cells. One-way ANOVA was performed and data are shown as mean ± *SD*; $F_{(236, 13)} = 13.99$, $n = 14$, $p < 0.0001$ (* symbols indicate comparisons of WT control vs. KO samples, §WT control vs. treated WT); significant differences identified by Bonferroni *post hoc* analysis are noted as follows: $^{*}p < 0.05$, $^{****\ §§§§}p < 0.0001$. (b) The average relative levels of Thr202/Tyr204-phosphorylated Mapk3/1 proteins (p-MAPK) in cerebellar primary astrocytes from *Gpr37l1*$^{+/+}$ or *Gpr37l1*$^{-/-}$ pups were determined as ratios to mean levels of total Mapk3/1 proteins (MAPK). Results are represented in arbitrary units normalized to average levels of p-MAPK observed in wild-type cultures (mean ± *SD*; $^{**}p < 0.009$ WT vs. KO, unpaired *t* test)

FIGURE S3 Original western blots. Entire original blots of Gpr37 (a), Gpr37l1 and Ptch1 (b), Shh (c, d) proteins. Dotted boxes indicate the portions used for figures 2d; 5c,d; 7b; 7c

Transparent Science Questionnaire for Authors

Transparent Peer Review Report

How to cite this article: La Sala G, Di Pietro C, Matteoni R, Bolasco G, Marazziti D, Tocchini-Valentini GP. Gpr37l1/prosaposin receptor regulates Ptch1 trafficking, Shh production, and cell proliferation in cerebellar primary astrocytes. *J Neurosci Res.* 2021;99:1064–1083. https://doi.org/10.1002/jnr.24775